Linking Dissolved Organic Matter Composition to Landscape Properties in Wetlands Across the United States of America

Martin R. Kurek[1,2] , **Kimberly P. Wickland**[3] , **Natalie A. Nichols**[4], **Amy M. McKenna**[5,6] , **Steven M. Anderson**[7] , **Mark M. Dornblaser**[8] , **Nikaan Koupaei-Abyazani**[9] , **Brett A. Poulin**[10], **Sheel Bansal**[11] , **Jason B. Fellman**[12] , **Gregory K. Druschel**[4], **Emily S. Bernhardt**[7], and **Robert G. M. Spencer**[1,2]

[1]Department of Earth, Ocean and Atmospheric Science, Florida State University, Tallahassee, FL, USA, [2]National High Magnetic Field Laboratory Geochemistry Group, Tallahassee, FL, USA, [3]U.S. Geological Survey, Geosciences and Environmental Change Science Center, Denver, CO, USA, [4]Department of Earth Sciences, Indiana University-Purdue University Indianapolis, Indianapolis, IN, USA, [5]National High Magnetic Field Laboratory Ion Cyclotron Resonance Facility, Tallahassee, FL, USA, [6]Department of Soil & Crop Sciences, Colorado State University, Fort Collins, CO, USA, [7]Department of Biology, Duke University, Durham, NC, USA, [8]U.S. Geological Survey, Water Resources Mission Area, Boulder, CO, USA, [9]Department of Atmospheric and Oceanic Sciences, University of Wisconsin-Madison, Madison, WI, USA, [10]Department of Environmental Toxicology, University of California, Davis, Davis, CA, USA, [11]U.S. Geological Survey, Northern Prairie Wildlife Research Center, Jamestown, ND, USA, [12]Alaska Coastal Rainforest Center and Department of Natural Sciences, University of Alaska Southeast, Juneau, AK, USA

Abstract Wetlands are integral to the global carbon cycle, serving as both a source and a sink for organic carbon. Their potential for carbon storage will likely change in the coming decades in response to higher temperatures and variable precipitation patterns. We characterized the dissolved organic carbon (DOC) and dissolved organic matter (DOM) composition from 12 different wetland sites across the USA spanning gradients in climate, landcover, sampling depth, and hydroperiod for comparison to DOM in other inland waters. Using absorption spectroscopy, parallel factor analysis modeling, and ultra-high resolution mass spectroscopy, we identified differences in DOM sourcing and processing by geographic site. Wetland DOM composition was driven primarily by differences in landcover where forested sites contained greater aromatic and oxygenated DOM content compared to grassland/herbaceous sites which were more aliphatic and enriched in N and S molecular formulae. Furthermore, surface and porewater DOM was also influenced by properties such as soil type, organic matter content, and precipitation. Surface water DOM was relatively enriched in oxygenated higher molecular weight formulae representing $HUP_{High\ O/C}$ compounds than porewaters, whose DOM composition suggests abiotic sulfurization from dissolved inorganic sulfide. Finally, we identified a group of persistent molecular formulae (3,489) present across all sites and sampling depths (i.e., the signature of wetland DOM) that are likely important for riverine-to-coastal DOM transport. As anthropogenic disturbances continue to impact temperate wetlands, this study highlights drivers of DOM composition fundamental for understanding how wetland organic carbon will change, and thus its role in biogeochemical cycling.

Plain Language Summary Dissolved organic matter (DOM) is often the most reactive form of organic carbon in wetlands, but its molecular characteristics and distribution are not well defined across different wetland types. We characterized DOM and analyzed dissolved organic carbon (DOC) concentrations across 12 temperate USA wetlands during wet and dry seasons from both surface- and porewaters. Wetland DOM primarily originates from the landscapes with greater DOC concentrations than similar inland waters such as lakes and rivers. DOM composition differs mostly by geographic site, suggesting that forested wetlands contain more aromatic DOM compounds from vegetation and soil than grassland/herbaceous wetlands, which contain DOM that is more processed. DOM composition between surface and porewaters is influenced by local ecological properties such as soil content and precipitation, with porewater compositions heavily impacted by mineral interactions. Finally, we identified common molecular signatures across all wetlands that have also been found in the largest arctic rivers, highlighting the role of wetlands as potential organic carbon sources to rivers and coastal systems. As precipitation and temperature patterns continue to change across temperate regions, the balance between different carbon pools will likely respond, particularly between the distribution and composition of wetland surface and porewater organic matter.

1. Introduction

Wetlands occupy only 4%–8% of Earth's land surface, but store 20%–30% (∼2,500 Pg) of the world's total soil carbon (C) within the first meter (Lal, 2008; Mitra et al., 2005). Wetlands provide important ecosystem functions for water quality management, wildlife refuge, flood control, and atmospheric C cycling (Ballard et al., 2013; Kolka et al., 2018; Mitra et al., 2005). Due to their frequent inundation and high productivity, wetland soils often experience prolonged anoxic conditions leading to anaerobic C respiration via alternate terminal electron acceptors, such as sulfate, and ultimately methanogenesis (Bridgham et al., 2013; D'Angelo & Reddy, 1999; Pester et al., 2012). Wetlands represent the largest natural source of atmospheric methane (CH_4) globally emitting between 101 and 179 Tg C yr^{-1} (Bridgham et al., 2013; Saunois et al., 2020). A significant portion (∼45 Tg C) of these CH_4 emissions occur across North American wetlands; however, their extent varies spatially with differences in soil type (mineral vs. organic) and vegetation cover (forested vs. non-forested; Kolka et al., 2018). In contrast, wetlands also have great potential for C storage in vegetation and soil, making their role as a C sink or source highly variable by region. For instance, North American wetlands store around 161–220 Pg C, with wetlands soils from the conterminous USA storing between 12 and 20 Pg C between various physiographic regions (Bridgham et al., 2006; Kolka et al., 2018; Nahlik & Fennessy, 2016). Due to the increased rate of anthropogenic greenhouse gas emissions and the high radiative forcing of CH_4, many wetlands do not currently sequester enough carbon dioxide (CO_2) to offset their CH_4 emissions, but over time some may become net C sinks (Bridgham et al., 2006; Mitsch et al., 2013). Therefore, understanding the composition and transfer between different wetland C pools will become increasingly important as inundation patterns change (Ballard et al., 2013; Easterling et al., 2017; Knapp et al., 2008) and anthropogenic land conversion mobilizes large stocks of soil C (Sanderman et al., 2017). Both of which are likely to expose wetland soils and increase CO_2 fluxes from weathering and decomposition (Bridgham et al., 2006; Kolka et al., 2018; Nahlik & Fennessy, 2016).

In addition to greenhouse gases, organic C is also an important component of wetland C cycling, potentially as both a C source and sink (Cole et al., 2007; Drake et al., 2018; Tranvik et al., 2009). Dissolved organic carbon (DOC), the commonly quantified subset of dissolved organic matter (DOM), can be laterally transferred across aquatic ecosystems via fluvial systems and serve as a common substrate for heterotrophic respiration, cycling terrestrial C back into the atmosphere (Battin et al., 2009; Tranvik et al., 2009; Zarnetske et al., 2018), or persisting in aquatic systems for extended periods depending on its intrinsic chemical properties and environmental constraints (Boye et al., 2017; Kellerman et al., 2018; Zark & Dittmar et al., 2018). Aquatic DOM represents a mixture of organic molecules from both terrestrial and internally produced sources and contains distinct chemical features that contribute to its function in aquatic ecosystems (Hansen et al., 2016; Kellerman et al., 2018; Rossel et al., 2013). For instance, DOM originating from fresh vegetation and algal biomass is considered highly biolabile on short timescales, while DOM that is more aromatic or has undergone extensive processing is typically less biolabile and respired over longer time scales (Guillemette et al., 2013; Hansen et al., 2016; Hensgens et al., 2021). In contrast, highly aromatic DOM is susceptible to photomineralization, which may degrade larger aromatic structures and produce smaller, more aliphatic molecules (Helms et al., 2008; Osburn et al., 2011). Furthermore, DOC concentrations and DOM composition in aquatic systems are heterogeneous and dependent on several external factors such as hydrology (Hanley et al., 2013; Zarnetske et al., 2018), climate and geomorphology (Hertkorn et al., 2016; Sobek et al., 2007), and landcover (Mann et al., 2014; Vaughn et al., 2021).

Due to the complexity of DOM mixtures, several analytical techniques are commonly utilized to identify and characterize specific components (e.g., D'Andrilli et al., 2022). Absorption spectroscopy has been used to identify and quantify bulk aromaticity in chromophoric dissolved organic matter (CDOM; Hansen et al., 2016; Helms et al., 2008; Weishaar et al., 2003), while fluorescence spectroscopy has been used to detect organic fluorophores within CDOM as well as quantify bulk properties using fluorescence-based indices (Fellman et al., 2010; Hansen et al., 2016; McKnight et al., 2001). Additionally, molecular-level DOM analysis has been conducted using Fourier-transform ion cyclotron resonance mass spectrometry (FT-ICR MS) to resolve mass differences between tens of thousands of individual molecular DOM formulae (Smith et al., 2018). FT-ICR MS analysis has been useful for identifying molecular degradation pathways (Kurek et al., 2020; Zark & Dittmar et al., 2018), characterizing non-chromophoric DOM components (Hertkorn et al., 2016; Kellerman et al., 2018), and quantifying bulk organic N and S (Kurek et al., 2020; Poulin et al., 2017). A combined approach utilizing bulk- and molecular-level analytical techniques has been useful in characterizing pools of organic C across boreal lakes (Johnston et al., 2020; Kurek et al., 2023), various soil types (O'Donnell et al., 2016; Ohno et al., 2014; Seifert et al., 2016),

rivers (Behnke et al., 2021; Jaffé et al., 2012), and can be utilized to compare DOM components across various wetlands.

Previous wetland DOM comparative studies have focused on systems from subtropical-tropical areas (e.g., Hertkorn et al., 2016; Mann et al., 2014; Poulin et al., 2017) or on the terrestrial fringes of hydrologically connected boreal lakes (e.g., Johnston et al., 2020; Kurek et al., 2023), but few, if any, have investigated across extensive temperature and precipitation regions of the USA. These regions, such as the Prairie Potholes (Dalcin Martins et al., 2017; Osburn et al., 2011; Sleighter et al., 2014), and the perhumid coastal temperate rainforest of southeast Alaska (D'Amore et al., 2015; Fellman et al., 2009, 2017), are important sources of terrestrial C, but their DOM composition has not been characterized in the context of other regional wetland sites. Furthermore, some past studies have characterized the DOM composition across broad regions from North American headwaters (Jaffé et al., 2008, 2012; Spencer et al., 2012), but largely omit the influence of wetlands, which are important contributors to lateral DOC and CDOM export (Hanley et al., 2013; Majidzadeh et al., 2017; Spencer et al., 2013; Zarnetske et al., 2018). Given the potential of wetlands to transfer large C pools, we present a novel assessment of DOC and DOM composition across a large climatic gradient of USA wetland sites, between surface waters, porewaters, and spanning wet, dry, and neutral hydroperiods.

The objectives of this study were: (a) to characterize DOC concentrations and DOM composition across various USA wetlands and to compare them to other well-studied wetlands (e.g., tropical-subtropical, boreal) as well as major riverine and lacustrine systems. (b) Compare differences in DOM composition between the different wetland sites within the context of geochemistry, hydrology, and landscape coverage. (c) Investigate differences between the vertical distributions of wetland DOM composition (surface vs. porewaters). As wetlands respond to changes in precipitation and temperature, their organic matter composition will likely also change, making this large-scale study important for future work investigating how anthropogenic climate and land use changes will affect wetland C cycling.

2. Materials and Methods

2.1. Study Sites and Field Sampling

Water samples ($n = 66$; Table S1) were collected from 12 wetland sites spanning various geographic regions of the United States (Figure 1; Table 1) at different hydrologic periods and depths from 2019 to 2021. Sampling locations were categorized based on National Wetlands Inventory classes (NWI; USFWS, 2021), land cover (NLCD; Dewitz & US Geological Survey, 2019), and dominant soil order (USDA STATSGO, 1994). Soil percent organic matter (OM) and top layer contents were obtained from the USDA Web Soil Survey (USDA-NRCS, 2019). Individual samples were grouped into local "wet," "dry," and "neutral" hydroperiods based on the Standardized Precipitation Index (SPI) calculated over the month prior to the sampling date (see Text S1 and Table S2 in Supporting Information S1; Table S1).

Water quality parameters including pH and specific conductivity (SpC) were measured using hand-held probes in the field. Samples were collected from standing surface water (surface water samples, $n = 36$) and soil porewaters (porewater samples, $n = 30$) 15 cm below the soil surface by drawing water through a perforated stainless steel rod under negative pressure. Both surface and porewater samples were filtered in the field through precombusted (450°C, >4 hr) 0.7 μm GF/F filters into acid-rinsed high-density polyethylene (HDPE) bottles. Two 15 mL aliquots were subsampled into separate bottles for Fe and dissolved sulfide analysis (see supplemental methods). Dissolved sulfide was preserved by adding 10% Zn acetate into the sample containers. Filtered samples were kept cold (4°C) and stored in the dark during transport and then frozen (−20°C) until analysis. Porewaters from the Florida Everglades were sampled slightly differently using a Teflon sipper and sulfide was measured by ion-selective electrodes (Tate et al., 2023).

2.2. DOC and Optical Analysis

Filtered water samples from wetlands were acidified (HCl, pH 2) and the DOC concentration was measured on a Shimadzu TOC-L CPH high temperature catalytic oxidation total organic carbon analyzer (Shimadzu Corp., Kyoto, Japan). Samples were sparged with air and DOC was quantified with a 5-point calibration curve following an established methodology (e.g., Kurek et al., 2020).
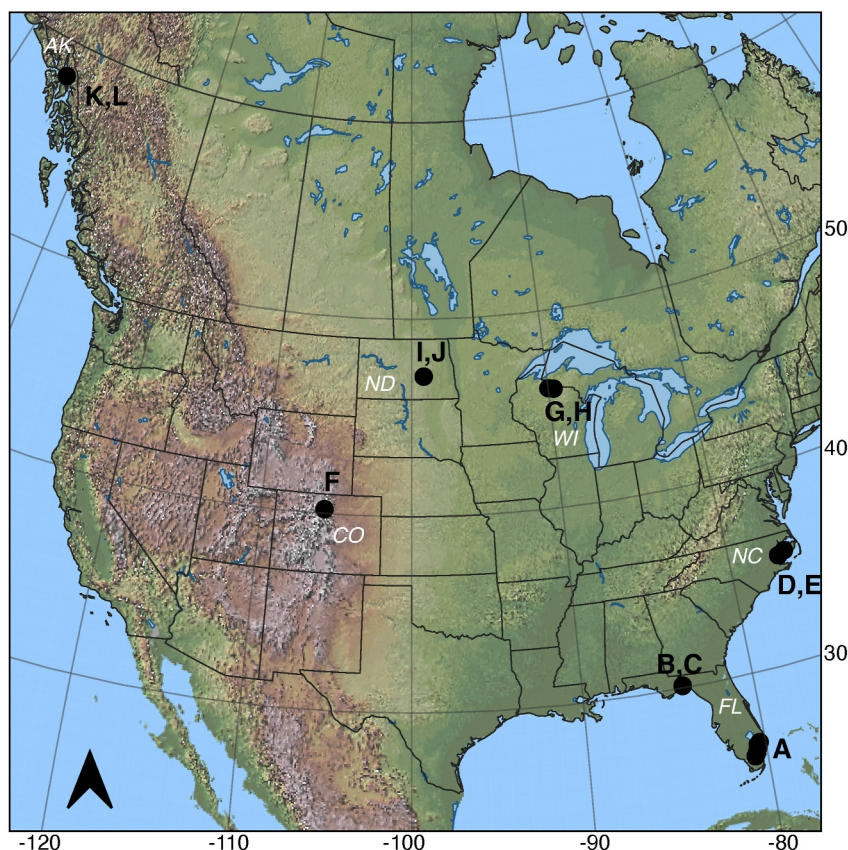
Figure 1. A map of the wetland sampling sites (black points, letters) and state names (white text) is described in Table 1. The base map is colored according to geographic relief with low relief denoted by green and increasing relief from yellow, brown, and white.

UV-vis absorbance spectra were measured at room temperature in a 1-cm quartz cuvette with a Horiba Scientific Aqualog (Horiba Ltd., Kyoto, Japan) at wavelengths of 230–800 nm. CDOM was determined as the Napierian absorption coefficient at 350 nm (a_{350}; m^{-1}). Spectral slopes have been related to aromaticity and molecular weight and were calculated from 275 to 295 ($S_{275-295}$; nm^{-1}) and 350–400 nm ($S_{350-400}$; nm^{-1}); the spectral slope ratio (S_R) was determined by dividing $S_{275-295}$ by $S_{350-400}$ (Helms et al., 2008). The ratio of absorbance at 250 and 365 nm (a_{250}:a_{365}), which is inversely proportional to aromaticity and molecular weight, was determined from absorbance spectra at 250 and 365 nm, respectively (Peuravuori & Pihlaja, 1997). Specific UV absorbance at 254 nm (SUVA$_{254}$; L mg C^{-1} m^{-1}) was related to CDOM content and was calculated by dividing the decadic absorption coefficient at 254 nm by the DOC concentration (mg L^{-1}; Weishaar et al., 2003).

Excitation-Emission matrices (EEMs) fluorescence spectra were also measured at room temperature in a 1-cm quartz cuvette using a Horiba Scientific Aqualog (Horiba Ltd., Kyoto, Japan). EEMs were collected at excitation wavelengths of 250–500 nm and emission wavelengths of 300–600 nm with 5 and 2 nm intervals, respectively, at integration times ranging from 0.2 to 10s. EEMs were corrected for lamp intensity (Cory et al., 2010), inner filter effects (Kothawala et al., 2013), and normalized to Raman units (Stedmon et al., 2003). Parallel factor analysis (PARAFAC) was modeled with 66 individual EEMs and validated using core consistency diagnostics and split-half validation (Murphy et al., 2013), producing a 5-component model that explained 99.82% of the variance. The model was compared to previously identified components using an online library (www.openfluor.org; Murphy et al., 2013). Finally, the fluorescence index (FI), which describes terrestrial and microbial contributions to DOM composition, was calculated from the emission intensity at 470 and 520 nm at excitation 370 nm (Cory & McKnight, 2005; McKnight et al., 2001).

Table 1
Wetland Sites, Geographic Sampling Locations, Wetland Type, Dominant Landcover, Annual Precipitation During Sampling Year, and Soil Properties

Site	State	Sampling location	Wetland type	Dominant landcover	Precipitation (mm)	Soil order	OM (%)	Top layer contents (0–15 cm)
A (n = 6)	FL	Everglades[a]	Freshwater Emergent	Emergent/Herbaceous	1,369	Histosol	75	Muck
B (n = 6)	FL	St. Marks National Wildlife Refuge	Freshwater forested and shrub	Woody wetlands	1,197	Alfisol	3	Sand
C (n = 6)	FL	St. Marks National Wildlife Refuge	Estuarine and Marine	Emergent/Herbaceous	1,197	Alfisol	14	Sand/mucky sand
D (n = 4)	NC	Goose Creek	Freshwater forested and shrub/Estuarine and Marine	Woody wetlands/Evergreen forests	1,249	Entisol/Alfisol	50	Muck
E (n = 4)	NC	Pocosin Lakes National Wildlife Refuge[b]	Freshwater forested and shrub (restored)	Pasture/Woody wetlands	1,048	Histosol	65	Muck
F (n = 5)	CO	Rocky Mountain National Park	Freshwater forested and shrub	Woody wetlands/Evergreen forests	958	Alfisol	39	Mucky peat, clay loam
G (n = 6)	WI	Little Bear Creek	Freshwater forested and shrub	Woody wetlands	819	Entisol	62	Muck
H (n = 6)	WI	Allequash Creek	Freshwater forested and shrub	Woody wetlands	819	Histosol	62	Muck
I (n = 5)	ND	Prairie Potholes	Freshwater emergent	Grassland/Herbaceous	480	Mollisol	2	Loam, clay loam
J (n = 6)	ND	Prairie Potholes	Freshwater emergent	Grassland/Herbaceous	480	Mollisol	8	Silty clay loam
K (n = 6)	AK	Douglas Island, Juneau	Freshwater forested and shrub	Evergreen forests	1,958	Histosol	80	Peat, sandy loam
L (n = 6)	AK	Douglas Island, Juneau	Freshwater forested and shrub/Freshwater Emergent	Evergreen forests	1,958	Histosol	95	Peat, muck

[a]Porewater samples were not collected from the Everglades. [b]Pocosin Lakes wetlands have been restored, which is not reflected in wetland type or landcover.

2.3. Solid Phase Extraction (SPE) and FT-ICR MS

Filtered water samples were acidified (HCl, pH 2) and extracted with Bond-Elut PPL columns (Agilent Technologies Inc., Santa Clara, CA) following established procedures (Dittmar et al., 2008). Columns were prepared by soaking with methanol (>4 hr), rinsing with methanol, and rinsing twice with Milli-Q water (pH 2). Approximately 50 μg C was isolated onto 100 mg 3 mL bed volume PPL columns (assuming at least 65% recovery), eluted with 1 mL methanol into precombusted (550°C, >4 hr) glass vials, and stored at −20°C until analysis. DOC recovery was assessed on several wetlands with duplicate extractions. Methanol extracts were collected in 40 mL glass vials and the methanol was evaporated by gently drying (50°C, overnight). The organic residue was redissolved in Milli-Q water (pH 2) and the DOC concentrations were measured using methods described in Section 2.2.

Methanolic extracts were analyzed on a custom-built hybrid linear ion trap ultra-high resolution FT-ICR mass spectrometer equipped with a 21T superconducting solenoid magnet at the National High Magnetic Field Laboratory (Tallahassee, FL; Hendrickson et al., 2015). Negatively charged ions from DOM were produced via electrospray ionization (ESI) at a flow rate of 500 nL min^{-1} conditionally co-added to yield 100 individual time-domain transients of 3.1 s each. Mass spectra were phase-corrected (Xian et al., 2010) and peaks were internally calibrated based on highly abundant O-containing series using a "walking" calibration (Savory et al., 2011) as described previously (e.g., Kurek et al., 2020). Further details regarding FT-ICR MS methodology are provided in the supplemental methods.

Mass spectral peaks (>6σ root-mean-square (RMS) baseline noise) were exported to a peak list and processed using PetroOrg © (Corilo, 2014). Molecular formulae were assigned to ions constrained by C_{4-75} $H_{4-150}O_{1-30}N_{0-4}S_{0-2}$ not exceeding 300 ppb error (e.g., Kurek et al., 2022). For all spectra, between 12,000 and 26,000 species were assigned elemental compositions with RMS error between 70 and 90 ppb and achieved resolving power >2,000,000 at m/z 400. Molecular formula properties, including the modified aromaticity index (AI_{mod}) and nominal carbon oxidation state (NOSC), were calculated according to Koch and Dittmar (2006, 2016) and Boye et al. (2017), respectively. Mass-weighted stoichiometric ratios were averaged (H/C, O/C, N/C, S/C) and formulae were also grouped based on the percent relative abundance of their heteroatoms (CHO, CHON, CHOS, and CHONS). Molecular formulae were grouped into compounds based on Šantl-Temkiv et al. (2013) including condensed aromatics (CA; $0.67 < AI_{mod}$), polyphenolics (PPh; $0.50 < AI_{mod} < 0.67$), highly unsaturated and phenolic low O/C ($HUP_{Low\ O/C}$; $AI_{mod} < 0.50$, H/C < 1.5, O/C < 0.5), highly unsaturated and phenolic high O/C ($HUP_{High\ O/C}$; $AI_{mod} < 0.50$, H/C < 1.5, 0.5 > O/C), and aliphatic (Ali; 1.5 < H/C), and the percent relative abundance of each class was summed.

2.4. Statistical Analysis

Data analysis including linear regression analysis and hypothesis testing ($\alpha = 0.05$ significance level) was performed in R (R Core Team, 2020) and visualized using the ggplot2 package (Wickham, 2016). A Principal Component Analysis (PCA) of the wetland sites according to their DOC and DOM properties was conducted with the factoextra package in R (Kassambara & Mundt, 2017). PARAFAC modeling was conducted in MATLAB using packages from Murphy et al. (2013).

3. Results

3.1. DOC Concentrations, Optical Parameters, and Geochemical Properties

DOC concentration and optical DOM properties spanned several orders of magnitude across the wetland sites, with no consistent differences between porewater and surface water or hydroperiod (Figure 2a). Most sites had DOC concentrations between 10 and 100 mg L^{-1}, while sites E and J had concentrations >100 mg L^{-1}, and a porewater sample from the Prairie Potholes (I) had a concentration of 4,930 mg L^{-1} (Figure 2a). CDOM absorbance at 350 nm (a_{350}) was between 10 and 100 m^{-1} in most samples while CDOM absorbance from sites E, I, and J was >100 m^{-1} (Figure 2b). $S_{275-295}$ ranged from 0.012 to 0.024 nm^{-1} at most sites but were consistently lower (0.012–0.015 nm^{-1}) in sites E, K, and L (Figure 2c). Other spectral slope parameters ($S_{350-400}$, S_R) and absorbance ratios (a_{250}:a_{365}) had similar trends to $S_{275-295}$ (Table S1). Finally, SUVA$_{254}$ values were between 1 and 4 L mg C^{-1} m^{-1} at most sites but notably higher at sites E, K, and L (Figure 2d).
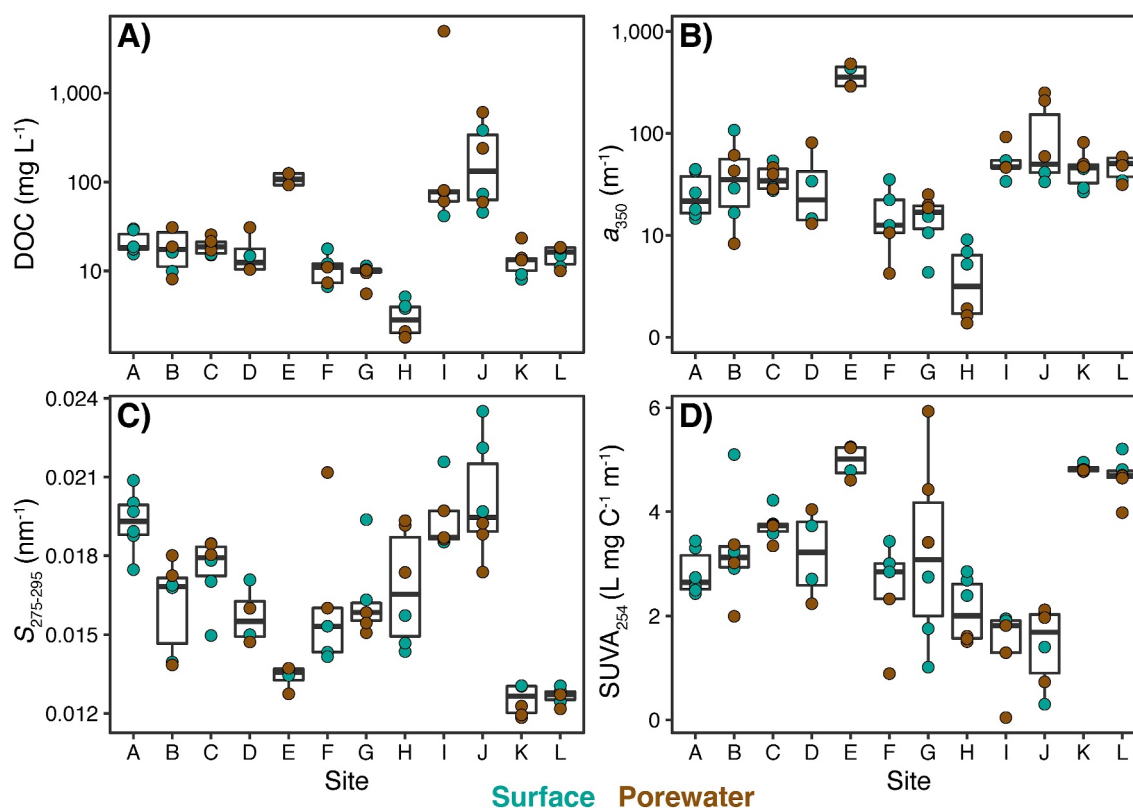
Figure 2. Boxplots of (a) Dissolved organic carbon, (b) CDOM absorbance (a_{350}), (c) $S_{275-295}$, and (d) SUVA$_{254}$ for wetland samples ordered by site. Colors indicate surface water samples (green) and porewater (brown). Sites are ordered along a latitudinal gradient from the southernmost sites (FL-EV, A) to the northernmost site (AK, L).

Similarly, SpC varied by several orders of magnitude with most sites between 100 and 1,000 µS cm^{-1}, while sites C, D, I, and J had SpC >1,000 µS cm^{-1} (Figure S1a in Supporting Information S1). Wetland pH was circum-neutral with most sites between 7 and 8 while sites E, K, and L were slightly acidic (4–6; Figure S1b in Supporting Information S1). Dissolved sulfide was significantly higher in porewater samples and nearly undetectable in surface waters (mean surface: 0.2 mg L^{-1}, mean porewater: 2.3 mg L^{-1}, $p < 0.05$), while Fe only varied slightly between depths (mean surface: 0.4, mean porewater: 1.0 mg L^{-1}, $p = 0.053$; Figures S1c and S1d in Supporting Information S1).

Wetland DOC concentrations were notably higher than in various North American headwaters (0.5–30 mg L^{-1}; Jaffé et al., 2008) river systems (1–46 mg L^{-1}; Hanley et al., 2013; Spencer et al., 2012) as well as subtropical wetlands (6.6–28.6 mg L^{-1}; Hertkorn et al., 2016; Poulin et al., 2017). In contrast, DOC concentrations were comparable to concentrations from forested North American boreal lakes (10–80 mg L^{-1}; Kurek et al., 2023). Optical aromaticity was similar to North American rivers in terms of $S_{275-295}$ (0.012–0.023 nm^{-1}; Spencer et al., 2012) but overall lower than in North American arctic-boreal lakes (0.012–0.030 nm^{-1}; Kurek et al., 2023). SUVA$_{254}$ was similar to North American rivers (1.3–4.7 L mg C^{-1} m^{-1}; Hanley et al., 2013; Spencer et al., 2012) and subtropical wetlands (2.7–5.1 L mg C^{-1} m^{-1}; Hertkorn et al., 2016) but slightly higher than in North American arctic-boreal lakes (0.5–4.0 L mg C^{-1} m^{-1}; Kurek et al., 2023).

3.2. SPE Recovery

SPE-DOC recoveries were assessed on a subset of wetland samples representative of the entire data set (ND1, FL4, AK1; Table S1). The average DOC recovery was 64.2 ± 4.6% for the three sites (ND1: 61.2 ± 0.7%, FL4: 67.5 ± 5.9%, AK1: 64.0 ± 5.7%) and comparable to recoveries measured from North American arctic-boreal lakes (52%–62%; Kurek et al., 2023) and riverine/coastal DOM (62%–65%; Dittmar et al., 2008). The high DOC recovery from these wetland sites suggests that the majority of DOM was extracted in PPL and could be
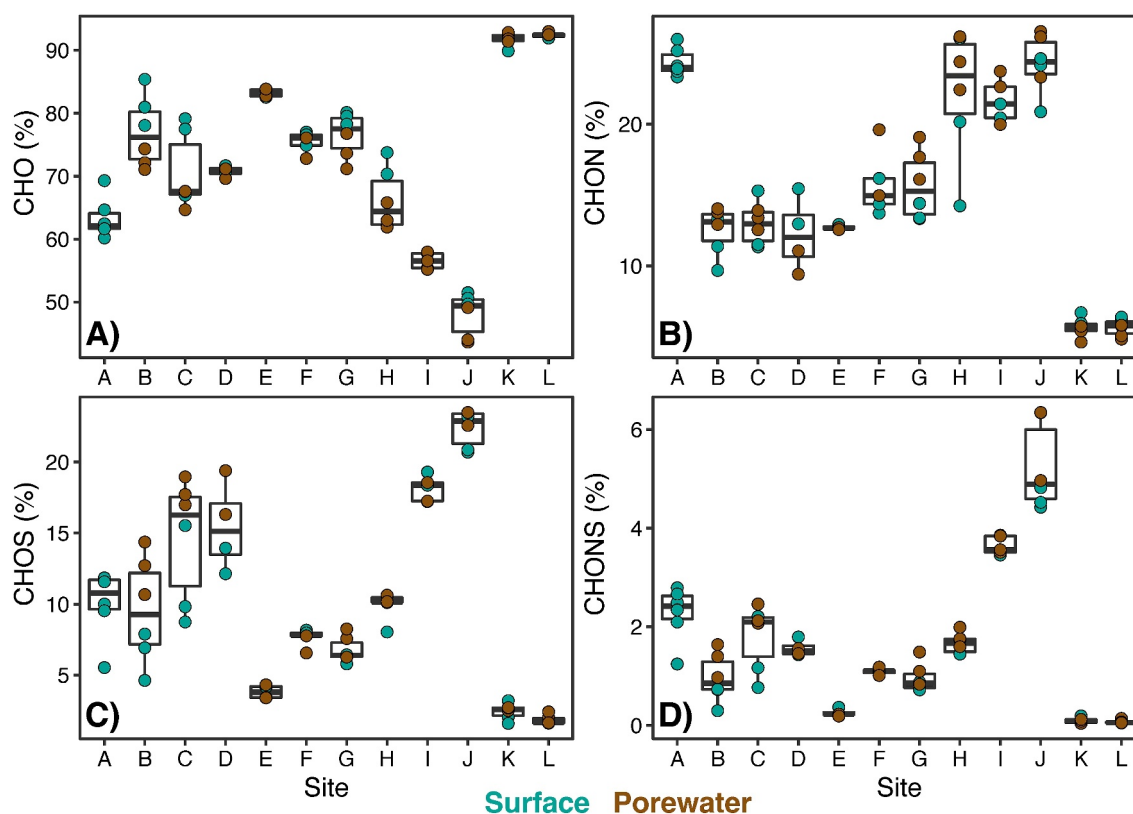
Figure 3. Boxplots of FT-ICR MS properties including the relative abundance (%) of formulae that are: (a) CHO-containing, (b) CHON-containing, (c) CHOS-containing, and (d) CHONS-containing for wetland samples ordered by site. Colors indicate surface water samples (green) and porewater (brown). Sites are ordered along a latitudinal gradient from the southernmost sites (FL-EV, A) to the northernmost site (AK, L).

represented in the FT-ICR MS spectra. Although approximately 30%–40% of DOC was not retained via PPL, SPE-DOM has been shown to be highly comparable across studies and proportional to bulk DOM optical and isotopic properties across diverse aquatic ecosystems (e.g., Kellerman et al., 2018; Kurek et al., 2023).

3.3. FT-ICR MS Properties

Heteroatom composition differed across wetland sites (Figure 3) with no consistent trends between surface water and porewater nor with hydroperiod. The greatest relative abundance included CHO-containing formulae (45%–90%, mean = 77.3%; Figure 3a), followed by CHON-containing formulae (5%–25%, mean = 15.6%; Figure 3b), CHOS-containing formulae (2%–25%, mean = 10.2%; Figure 3c), and CHONS-containing formulae having the lowest relative abundance (0%–6%, mean = 1.7%; Figure 3d). Sites K and L were the most relatively depleted in heteroatoms (Figure 3a), while sites A, H, I, and J were the most relatively enriched in N and S formulae (Figures 3b–3d).

Similarly, the relative abundance of molecular compound classes did not follow consistent trends between surface water and porewater nor between hydroperiod. Instead, inferred compound classes varied by wetland site (Figure 4). $HUP_{High\ O/C}$ formulae had the greatest relative abundance (35%–65%, mean = 52.7%; Figure 4b), followed by $HUP_{Low\ O/C}$ formulae (25%–40%, mean = 27.0%; Figure 4c), CA + PPh formulae (5%–25%, mean = 14.5%; Figure 4a), and aliphatic formulae having the lowest relative abundance (2%–14%, mean = 5.9%; Figure 4d). Sites E, K, and L were enriched in aromatic and $HUP_{High\ O/C}$ formulae (Figures 4a and 4b) and had a lower relative abundance of aliphatic and $HUP_{Low\ O/C}$ formulae (Figures 4c and 4d). Furthermore, these sites had fewer assigned molecular formulae (Figure S2a in Supporting Information S1), which had greater average molecular weights (Figure S2b in Supporting Information S1), aromaticity (Figures S2c and S2e in Supporting Information S1), and oxygenation (Figures S2d and S2f in Supporting Information S1).
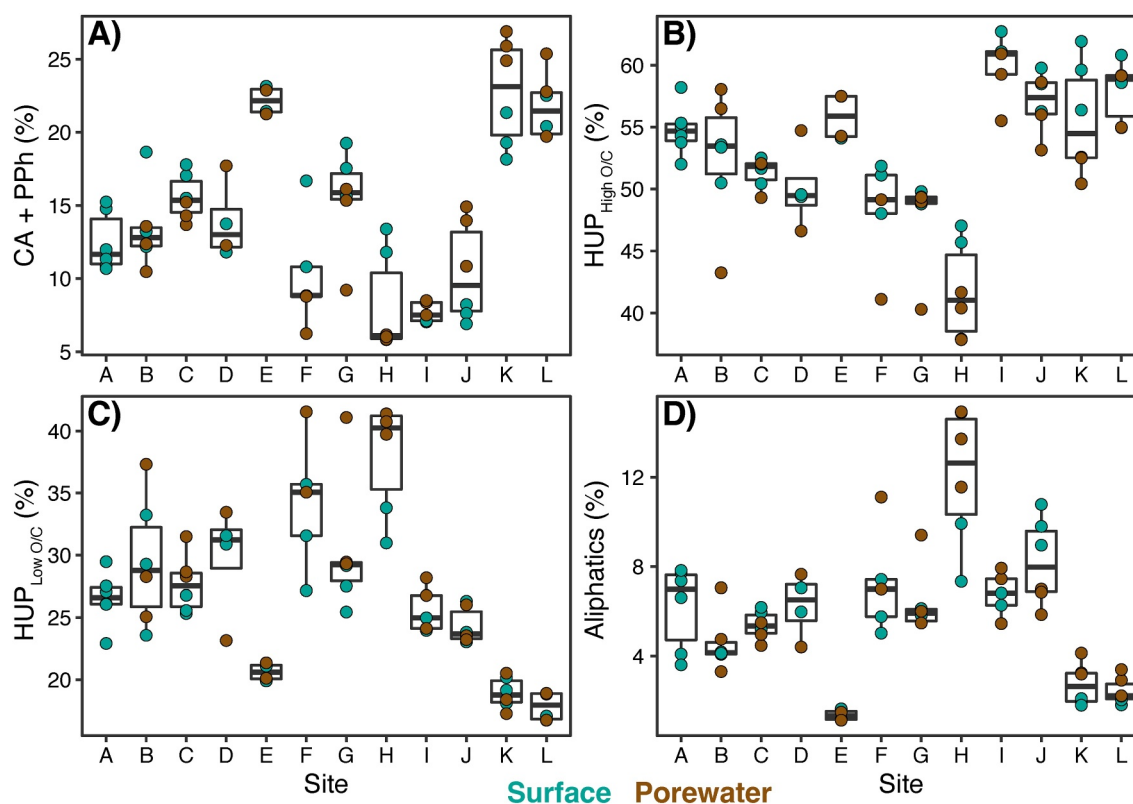
Figure 4. Boxplots of FT-ICR MS properties including the relative abundance (%) of formulae that are: (a) condensed aromatic and polyphenolic (CA + PPh), (b) highly unsaturated and polyphenolic high O/C ($HUP_{High\ O/C}$), (c) highly unsaturated and polyphenolic low O/C ($HUP_{Low\ O/C}$), and (d) Aliphatics for wetland samples ordered by site. Colors indicate surface water samples (green) and porewater (brown). Sites are ordered along a latitudinal gradient from the southernmost sites (FL-EV, A) to the northernmost site (AK, L).

Heteroatom distributions in wetland samples were similar to North American arctic-boreal lakes (Kurek et al., 2023) and temperate coastal Chinese wetlands (Lu et al., 2020) but had a lower relative abundance of CHON than subtropical wetlands (20%–35%; Hertkorn et al., 2016). Wetland samples from this study were also more aromatic, as evident from the greater relative abundance of CA + PPh formulae (6%–26%) compared to arctic-boreal lakes (5%–15%; Kurek et al., 2023) and temperate coastal Chinese wetlands (1%–5%; Lu et al., 2020). Finally, molecular aliphaticity in wetlands from this study were slightly higher than in subtropical wetlands (H/C: 1–1.1; Hertkorn et al., 2016; Figure S2c in Supporting Information S1), while oxygenation was comparable between the studies (O/C: 0.46–0.56; Hertkorn et al., 2016; Figure S2d in Supporting Information S1).

3.4. Molecular-Level Signatures

Molecular formulae that were common across all samples (denoted as wetland$_{Common}$) including each geographic state and water depth were identified and their average atomic stoichiometries were calculated (Figure 5; Table S3 in Supporting Information S1). We identified 3,489 unique peaks common across all 66 wetland mass spectra consisting of CHO-, CHON-, and CHOS-containing formulae (Figure 5a). These formulae were then compared to formulae from the Core Arctic Riverine Fingerprint (CARF), which is a group of 1,328 individual formulae identified in the six largest arctic rivers across various years and hydroperiods and is thought to represent a stable source of organic C to marine systems (Behnke et al., 2021). From this subset, we found 1,255 CARF formulae (~95%) common in all wetland samples, including surface water and porewater, which were slightly more saturated (higher H/C) than the wetland$_{Common}$ formulae (Figure 5b).

Next, using the wetland$_{Common}$ formulae, we identified peaks that had consistently greater mean normalized abundances in surface water samples and porewater samples, respectively. Peaks that were more abundant in surface water samples ($n = 1,588$) were more oxygenated (higher O/C; Figure 5c) and had mass distributions
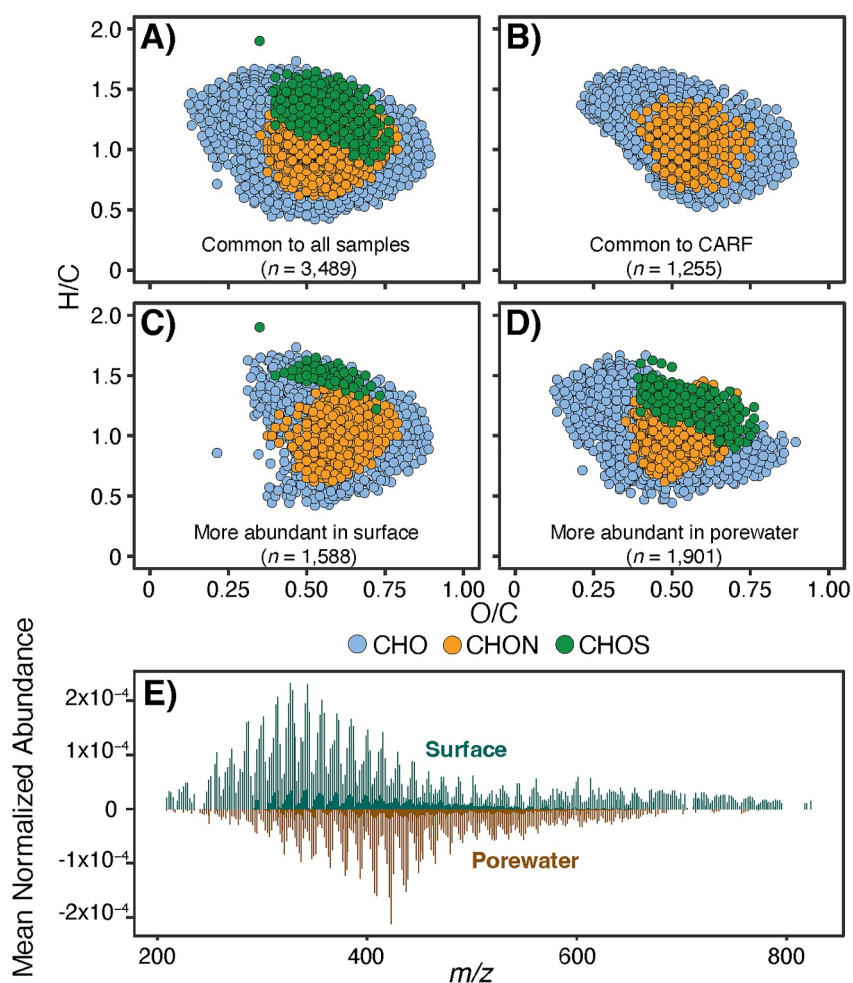
Figure 5. van Krevelen diagrams of molecular formulae (a) found in all samples, (b) found in all samples that are also found in the Core Arctic Riverine Fingerprint (CARF; Behnke et al., 2021), (c) more abundant in surface water spectra than in porewater spectra, and (d) more abundant in porewater spectra than surface water spectra. Points are colored according to their heteroatomic composition (CHO-containing, blue; CHON-containing, orange; CHOS-containing, green). (e) mass spectra of peaks with a greater mean normalized abundance in surface water samples (positive peaks, green) and peaks with a greater mean normalized abundance in porewater samples (negative peaks, brown).

skewed to lower mass ($m/z < 400$) as well as tail extending to higher masses ($700 < m/z < 800$; Figure 5e). In contrast, peaks which were more abundant in porewaters ($n = 1,901$) had less oxygenation similar to $HUP_{Low\ O/C}$ formulae and greater CHOS content (Figure 5d) with a more Gaussian mass distribution centered around $m/z = 400$ (Figure 5e).

3.5. PARAFAC Modeling

PARAFAC analysis of the wetland sites yielded a five-component model (Figure S3 in Supporting Information S1), which was validated through split-half analysis (Figure S4 in Supporting Information S1). The five components (C1–C5) were compared with other DOM fluorophores using the online library OpenFluor based on their greatest percent similarity (Murphy et al., 2013). C1 ($Ex_{240,340}$, Em_{442}) was similar to terrestrial fluorophores in treated wastewater (Moona et al., 2021), "humic-like" fluorophores in sea ice (Stedmon et al., 2007), and correlated positively with parameters linked to aromatic DOM (Table S4 in Supporting Information S1). C2 ($Ex_{270,385}$, Em_{504}) was similar to terrestrial fluorophores from surface waters (Wünsch et al., 2017), treated wastewater (Moona et al., 2021), and also correlated positively with parameters linked to aromatic DOM (Table S3 in Supporting Information S1). C3 ($Ex_{240,310}$, Em_{395}) was similar to "fulvic-like" fluorophores from aquaculture DOM (Gullian-Klanian et al., 2021), recently processed terrestrial fluorophores (Moona et al., 2021), and
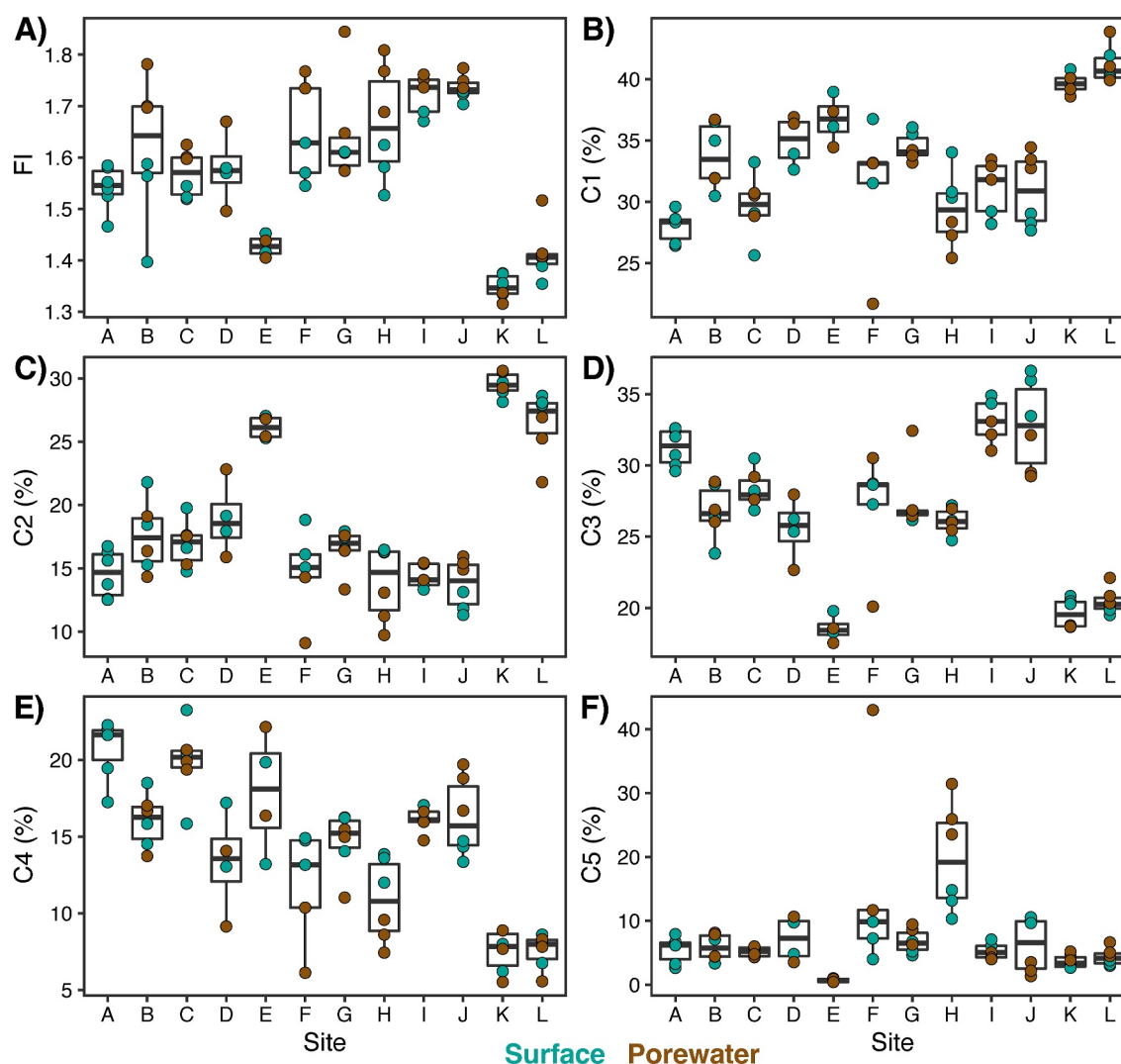
Figure 6. Boxplots of FDOM properties including: (a) Fluorescence Index, (b) %C1, (c) %C2, (d) %C3, (e) %C4, and (f) %C5 for wetland samples ordered by site. Colors indicate surface water samples (green) and porewater (brown). Sites are ordered along a latitudinal gradient from the southernmost sites (FL-EV, A) to the northernmost site (AK, L).

correlated positively with aliphaticity and heteroatom-content (Table S4 in Supporting Information S1). C4 (Ex_{250}, Em_{450}) was similar to "humic-like" fluorophores in DOM from lake ice (Imbeau et al., 2021), fluorophores from tropical peatlands (Zhou et al., 2019), and correlated positively with DOC and heteroatom-content (Table S3 in Supporting Information S1). Finally, C5 (Ex_{275}, Em_{325}) was similar to protein-like fluorophores from wetlands (Yamashita et al., 2010), streams (Graeber et al., 2021), and correlated positively with aliphaticity and %CHON (Table S4 in Supporting Information S1).

3.6. FDOM Composition

FDOM composition varied mostly by wetland site, with the exception of FI, which was significantly higher in porewaters than surface waters (mean surface = 1.54, mean pore = 1.62, $p < 0.05$; Figure 6a). Wetland FI values were similar to DOM from various North American headwaters (1.1–1.8; Jaffé et al., 2008) and North American arctic-boreal lakes (1.3–1.7; Kurek et al., 2023), but higher than in subtropical wetlands (1.3–1.4; Hertkorn et al., 2016). C1 was on average the dominant component ranging from 25% to 45% (mean = 33.4%; Figure 6b), followed by C3 (20%–35%, mean = 26.6%; Figure 6d), C2 (10%–30%, mean = 18.5%; Figure 6c), C4 (5%–20%, mean = 14.3%; Figure 6e), and C5 with the lowest proportion (1%–12%, mean = 7.2%; Figure 6f). FI was notably
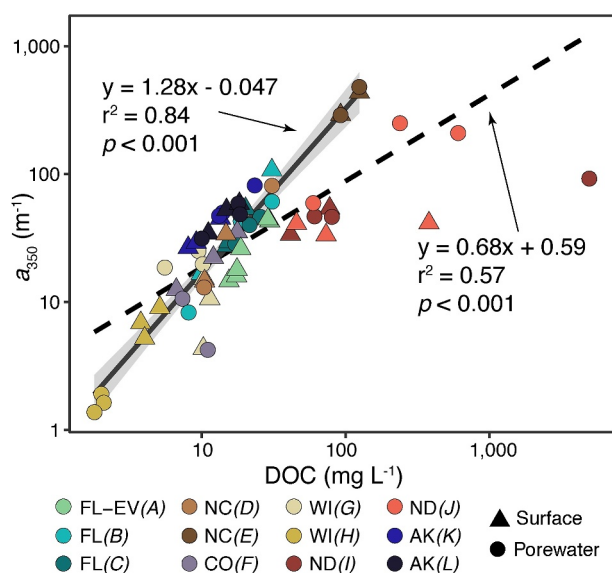
Figure 7. Relationship between dissolved organic carbon and chromophoric dissolved organic matter absorbance at 350 nm (a_{350}) across all wetland sites. Samples are denoted by surface water (triangles) and porewater (circles) and colored according to their geographic state and sampling site. Dashed line represents the linear regression of all samples while the solid line represents the linear regression of all samples except for ND. Shading around the solid line describes the 95% confidence interval.

lower and terrestrial fluorophores were higher at sites E, K, and L, while protein-like fluorophores were higher in sites F and H (Figure 6). There were no consistent trends between FDOM composition and hydroperiod.

4. Discussion

4.1. Properties of Wetland DOM

This study encompasses a continental range of wetland DOM properties including DOC, optical properties (absorbance, fluorescence), and molecular composition (FT-ICR MS analysis) revealing differences in DOM cycling between wetlands and other inland aquatic systems. DOC concentrations and DOM composition were distinct to each sampling site and varied over the course of the sampling year (hydroperiods) and by depth (surface water vs. porewater) by geographic differences in soil properties, vegetation, and precipitation.

These comparisons highlight that wetlands contain some of the highest DOC concentrations compared to other inland aquatic systems and incorporate terrestrial DOM from the surrounding landscape, much like North American rivers and several tropical-subtropical wetlands (e.g., Hertkorn et al., 2016; Spencer et al., 2012). Strong coupling of DOC to terrestrial DOM is supported by the positive correlation of DOC with a_{350} (Figure 7), which is similar to North American (Spencer et al., 2012) and central African rivers (Lambert et al., 2015). Despite their similarities, these temperate USA wetlands differ from the subtropical-tropical wetlands in their higher FI values (Hertkorn et al., 2016; Mann et al., 2014), suggesting differences in microbial and

aquatic DOM sourcing (Fellman et al., 2010; Hansen et al., 2016; McKnight et al., 2001). Most temperate wetlands from this study likely undergo cycles of inundation and drying, where terrestrial DOM (low FI values) accumulates during periods of high precipitation and is subsequently degraded and mixed with internally produced DOM (high FI values) during receding water. This is further supported by the positive correlation of FI with %C3 ($r^2 = 0.53$, $p < 0.001$) suggesting higher FI is related to processed and reworked aromatic DOM. In contrast, large tropical wetlands, such as the Amazon and Congo, are permanently inundated and connected to river systems with little changes to the water level (Prigent et al., 2007). In these wetlands, as well as southeast Alaska (sites K and L), terrestrial DOM is constantly supplied from surrounding vegetation and flushed into connected fluvial systems, resulting in highly aromatic DOM with low FI values and limited mixing with internally produced DOM sources.

Across all wetland sites and hydroperiods, we identified a set of highly abundant molecular formulae in each sample, wetland$_{Common}$, across both porewater and surface waters (Figure 5a; Table S3 in Supporting Information S1). This group includes a network of oxygenated CHON-containing formulae (O/C: 0.4–0.8) that has been identified across several tropical-subtropical wetlands, as well as a cluster of saturated CHOS-containing formulae (H/C: 0.9–1.6) more prevalent in the Florida Everglades (Hertkorn et al., 2016; Poulin et al., 2017). The diversity of these persistent N and S-containing formulae across all the wetlands suggests a commonality of degradation processes during DOM transport, despite the differences in terrestrial and aquatic sourcing between sites and sampling depths (e.g., Hensgens et al., 2021; Rossel et al., 2013). Furthermore, the PPL-extractable fraction mostly represents nonpolar to polar hydrophobic acids and omits lower molecular weight and hydrophilic species, which are typically more saturated (Li et al., 2017; Raeke et al., 2016). This likely means that wetland DOM is far more diverse across sites and between sampling depths, and the utilization of complimentary isolation procedures may reveal additional differences in DOM composition such as sourcing and inferred biolability. Regardless, DOM parameters from the PPL-fraction are proportional to bulk properties (Table S4 in Supporting Information S1) and represent high molecular-level commonality across other studies.

Such commonality is consistent with findings from other broad scale DOM studies of inland waters (e.g., Behnke et al., 2021; Jaffé et al., 2012). For instance, within the wetland$_{Common}$ formulae, we find over 95% of the CARF formulae from the six largest Arctic rivers, which are exported to marine systems (Behnke et al., 2021; Figure 5b). The high commonality of the CARF formulae within these wetland samples provides further support for their
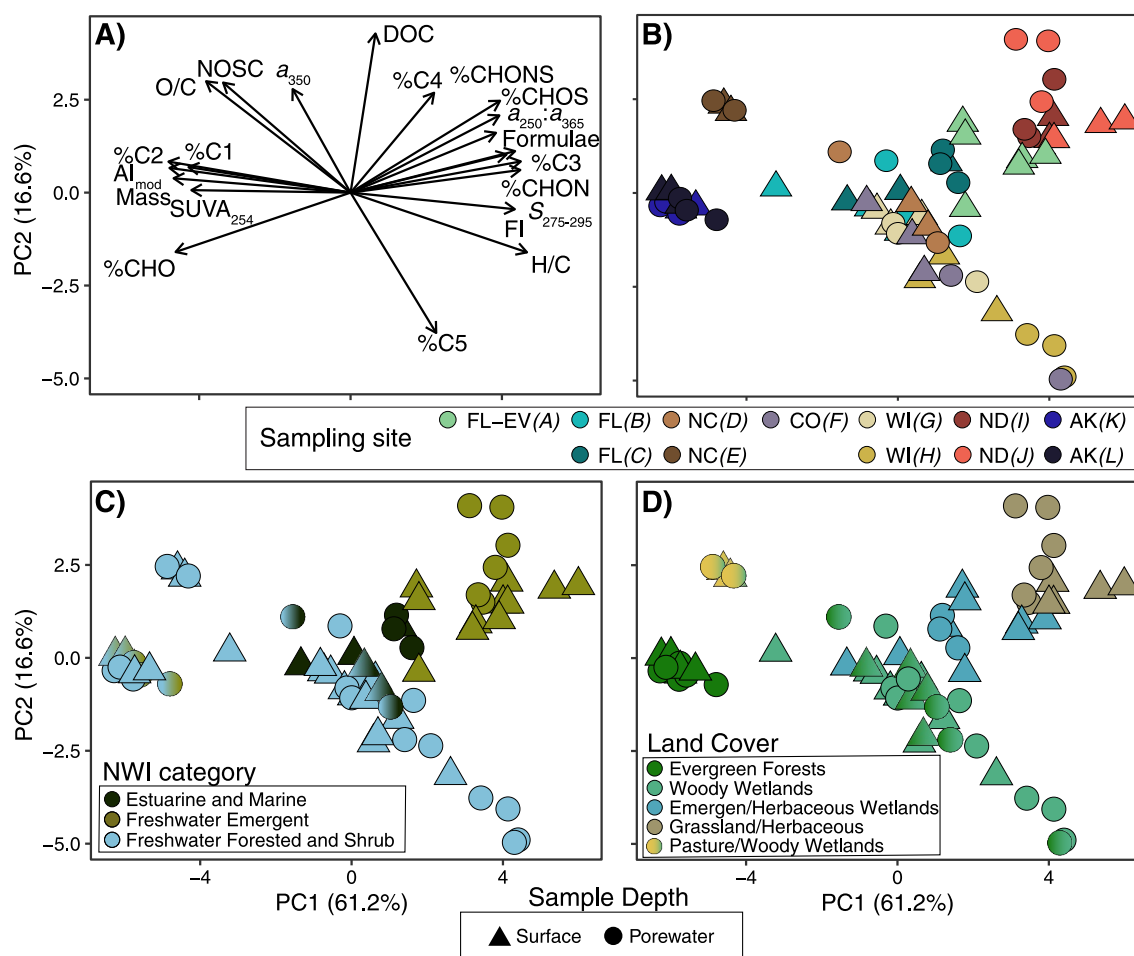
Figure 8. Principal component analysis biplot (PC1 vs. PC2) of dissolved organic carbon (DOC) and dissolved organic matter (DOM) properties via absorbance, fluorescence, and FT-ICR MS analysis. (a) DOC and DOM variables are represented as solid vectors. Symbols are colored according to: (b) geographic and sampling site, (c) NWI wetland category (USFWS, 2021), and (d) dominant land cover. Wetland samples are denoted by surface water (triangles) and porewater (circles). Note: shapes with a color gradient represent significant influence of both corresponding categories.

stability and that wetlands connected to riverine systems could be an important C source for marine DOM. However, these compositional trends differ slightly when compared to major tropical rivers with wetland influence (e.g., Amazon, Congo River). Wetland$_{Common}$ formulae were in similar mass ranges to molecular formulae found in both the Amazon and Congo River, but wetland$_{Common}$ CHO and CHON-containing formulae had higher average O/C ratios, possibly reflecting differences in tropical soil organic matter and processing during transport in higher Strahler order rivers (Figure 5a; Kurek et al., 2022). Although we recognize that these molecular formulae likely represent thousands of individual isomers, DOM formulae from marine and freshwater systems have been shown to share many structural features that represent common degradation mechanisms and can be useful for identifying common pathways in aquatic DOM cycling (Zark & Dittmar, 2018).

4.2. Drivers and Sources of Wetland DOM Composition

A principal components analysis (PCA) was conducted to visualize trends in DOM composition and how they relate to sites, wetland types, sampling depth and landcover (Figure 8). Two components (PC1 and PC2) explained 77.8% of the variance between all the samples. PC1 (61.2%) correlated positively with $S_{275-295}$, FI, H/C, %CHON, and %C3 and negatively with SUVA$_{254}$, AI$_{mod}$, Mass, %CHO, %C1, and %C2 (Figure 8a). This suggests that PC1 relates to aromaticity and processing where negative values (PC1 < 0) indicate greater aromaticity and molecular stability from higher molecular-weight terrestrial fluorophores, while positive values (PC1 > 0) indicate input from more diverse non-aromatic DOM sources as well as photochemical and microbial

processing. In contrast, PC2 (16.6%) correlated positively with DOC, NOSC, O/C, %C4, and a_{350} and negatively with %C5 (Figure 8a), suggesting that it was related to terrestrial bulk organic matter quantity. Positive values (PC2 > 0) denote samples with greater DOC concentrations, which tend to originate from oxidized terrestrial sources, while negative values (PC2 < 0) denote samples with lower DOC, which tend to be depleted in terrestrial DOM but enriched in protein-like fluorophores.

We did not observe any consistent trends with the DOM composition and hydroperiod in the principal component space as there was extensive overlap on both axes between the wet, dry, and neutral hydroperiods (Figure S5 in Supporting Information S1). Similarly, wetland samples did not separate by sampling depth and instead clustered together mostly by sampling site, wetland type, and dominant landcover, which was illustrated by differences in forested and emergent/herbaceous vegetation (Figure 8). The greatest separation was between two clusters of sites along PC1: E, K, L (forested and pasture sites) and I, J, A (grassland and herbaceous sites; Figure 8). This separation corresponds to a gradient of SpC and pH values where the two clusters represent opposite compositional endmembers in PC1 as well as upper and lower ranges in SpC and pH values, resulting in a significant inverse relationship between aromaticity with SpC and pH (Figure S6 in Supporting Information S1).

The samples with the lowest SpC and pH (sites E, K, L) represent forested and shrub-dominated wetlands with DOM that is highly aromatic, oxidized, and depleted in N, S-content (Figure S6 in Supporting Information S1, Figure 8c). Their composition was similar to DOM from leaf litter and forested riverine catchments, particularly in their enrichment of condensed aromatic and polyphenolic formulae (15%–23%; Textor et al., 2018; Vaughn et al., 2021). Furthermore, the Pocosin Lakes wetlands (E) are surrounded by a mixture of pastures, forests, and rewetted peatlands, while sites from southeast Alaska (K, L) are also underlain by organic-rich peat but surrounded by evergreen forests (Figures 8d and Table 1). These were also similar to CDOM leached from organic rich surface soils (Hansen et al., 2016; Seifert et al., 2016) as well as condensed aromatic and polyphenolic formulae from forested soil organic matter (20%–30%; O'Donnell et al., 2016; Ohno et al., 2014). Their compositional similarity to forested vegetation suggests that the forested wetland DOM is highly terrestrial and originates from the landscape during periods of inundation (Fellman et al., 2009; Majidzadeh et al., 2017). As these wetland sites had overall higher soil organic matter content and percent organic matter than the grassland and herbaceous sites (Figure S7 in Supporting Information S1), it is likely that much of their aromatic DOM also originated from hydrologically connected soils. Furthermore, while DOM from both sites is highly aromatic, site E has higher DOC and bulk CDOM than the southeast Alaska sites (Figure 2), suggesting that anthropogenically impacted wetlands could serve as a significant source of DOC to surrounding surface waters.

In contrast, sites I, J, and A had the highest SpC and pH, representing freshwater emergent wetlands/grasslands with more aliphatic DOM, microbial fluorophores, and N,S-content (Table 1; Figure 8). This distinct clustering suggests this DOM is more processed and originates from non-forested landscapes (Jaffé et al., 2012; Rossel et al., 2013; Seifert et al., 2016) and vegetation such as grasses, bulrush, and macrophytes whose leachates are also relatively enriched in aliphatics (16%–30%; Johnston et al., 2019). Furthermore, DOM from sites I, J, and A, as well as the estuarine and marine sites (C,D), are enriched in CHOS formulae which have also been identified in other DOM samples from the Prairie Potholes and Florida Everglades (7%–38%; Dalcin Martins et al., 2017; Hertkorn et al., 2016; Poulin et al., 2017; Sleighter et al., 2014). The high relative abundance and unique distributions of these CHOS formulae likely originate from abiotic sulfurization reactions between terrestrial DOM and reduced sulfur species (e.g., inorganic sulfide). These inorganic sulfides are produced in anoxic porewaters via microbial sulfate reduction of groundwater or seawater sulfate (Pester et al., 2012).

Abiotic sulfurization is further supported by relatively higher dissolved sulfide concentrations at sites A, C, D, I, and J (Figure S1c in Supporting Information S1), which are comparable to previous studies of the Florida Everglades (Poulin et al., 2017) and Prairie Potholes (Dalcin Martins et al., 2017). Additionally, anoxia preserves reduced organic matter in floodplain porewaters as more oxidized compounds are respired during sulfate reduction (Boye et al., 2017). Thus, the combination of organic matter sulfurization and slow DOM degradation rates in anoxic waters may be an important mechanism for organic carbon preservation in similar wetland sites (Lu et al., 2020), resulting in unique CHOS distributions.

Finally, differences in DOM sourcing along PC1 are illustrated in Figure 7, where the DOC-a_{350} regression slope becomes shallower and the overall relationship is weaker (lower r^2) after including the Prairie Pothole sites (I, J). This is likely due to the low soil organic carbon and organic matter content of these soils (Figure S7 in Supporting Information S1), which limit the overall availability of aromatic organic matter for transport. Furthermore, limited

precipitation (Table 1) restricts the input of terrestrial organic matter from the soils and evaporation concentrates solutes such as internally produced DOC in surface waters (Figure 2a; Figure S1a in Supporting Information S1). Prolonged water residence removes aromaticity via photodegradation, resulting in steeper spectral slopes (Figure 2c) and lower SUVA$_{254}$ (Figure 2d), while DOC was replenished from autochthonous production and subsurface microbial sources as suggested by high FI values (Figure 6a), C3 fluorescence (Figure 6d), and pH (Figure S1b in Supporting Information S1). Diverse organic matter sourcing in the Prairie Potholes also agrees with previous studies that reported high DOC concentrations, autochthonous signatures, low lignin yields (i.e., limited vascular plant contributions), and microbial fluorescent peaks (Dalcin Martins et al., 2017; Osburn et al., 2011) and may serve as a compositional endmember for similar emergent wetlands in semiarid climates and grasslands.

4.3. Differences Between Surface Water and Porewater DOM

Porewaters had significantly higher FI values (Figure 6a), sulfide (Figure S1c in Supporting Information S1), and Fe (Figure S1d in Supporting Information S1) than surface waters. These differences suggest that wetland porewaters experience more dynamic redox conditions where microorganisms utilize alternate terminal electron acceptors (e.g., sulfate, Fe) to oxidize thermodynamically favorable DOM compounds, while reduced DOM molecular formulae (i.e., lower NOSC) are preserved (Boye et al., 2017; Lau & del Giorgio, 2020). Molecular formulae that are more abundant across all the surface waters are generally more oxygenated (higher O/C) and exhibit a non-Gaussian mass distribution that extends to higher masses (Figures 5c and 5e). This suggests that wetland DOM is dominated by higher molecular-weight terrestrial polymers that are processed and result in a distribution of lower molecular weight and oxidized DOM formulae, as has been identified in other terrestrial surface waters (Aukes & Schiff, 2021; Mann et al., 2014). In contrast, molecular formulae that are more abundant in porewaters follow a more Gaussian distribution centered on medium masses and are shifted to lower O/C values with greater diversity of N- and S-containing formulae (Figures 5d and 5e). These formulae are likely sourced from microbial exudation and continuous degradation of soil and plant-derived biopolymers (Lehmann & Kleber, 2015), both of which have been shown to afford similar DOM compositions (Hensgens et al., 2021; Roth et al., 2019).

In contrast to these findings, previous studies have reported significant differences in DOM molecular composition between depths. For instance, studies of Canadian freshwaters have identified significantly greater aromaticity and higher molecular weight in porewater DOM compared to the overlying water (Aukes & Schiff, 2021; Prijac et al., 2022); however, porewaters from these sites were collected at greater depths (50 cm) than in this study (15 cm). The shallow depth and vertical connectivity of surface waters with porewaters from this study is further illustrated by the nearly identical DOM molecular composition of formulae common to porewaters with the formulae common to all surface waters (Table S3 in Supporting Information S1). This similarity contrasts with DOM observed in deep peat columns (50–200 cm), which undergo various biogeochemical processing due to their vertical stratification (Tfaily et al., 2018). Furthermore, it is possible that our individual spot sampling did not capture the average DOM molecular compositions at each site, which is influenced by soil layer depths, organic horizon extent, and mineral surface adsorption (Lehmann & Kleber, 2015; Roth et al., 2019). To illustrate, porewaters from Chinese coastal wetlands were sampled from homogenized sediments and displayed significantly greater aromaticity and S-content than DOM from the overlying water (Lu et al., 2020).

Finally, these wetland study sites represent diverse ecological and pedological zones, each with geochemical constraints on subsurface organic matter. For instance, precipitation events will saturate pore spaces and increase vertical connectivity with surface waters, transporting DOC and nutrients (D'Amore et al., 2015), while creating intermittent periods of anoxia (Knapp et al., 2008). In contrast, drying increases the exposure of surface and subsurface soil organic matter to oxygen (Knapp et al., 2008). Differences in soil mineralogy also likely account for the inconsistency of porewater DOM composition between sites. For example, the lower aromaticity in the forested FL (B) porewaters than surface waters could be due to the high Fe oxide and clay content of the surrounding alfisols. These minerals preferentially adsorb oxygenated and aromatic DOM compounds, excluding them from the porewater solution (Groeneveld et al., 2020; Riedel et al., 2013).

4.4. Future Outlook

There is great uncertainty regarding how the biogeochemistry of temperate USA wetlands will respond to future climate scenarios as C storage and transport are highly dependent on landcover and soil content (Kolka
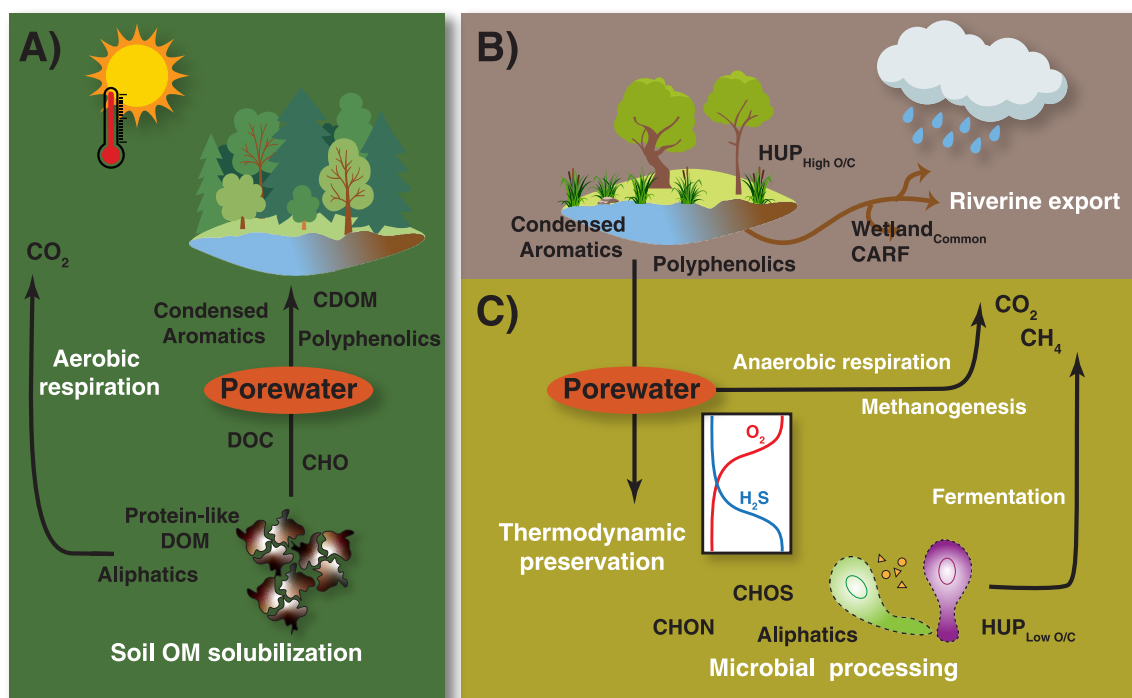
Figure 9. Conceptual diagram of wetland dissolved organic matter (DOM) responses from this study to projected changes in warming and precipitation. (a) Under warming conditions in forested wetlands, dissolved organic carbon and chromophoric dissolved organic matter will be released from soil organic matter and accumulate in porewaters and well-connected surface waters. Higher temperatures will lead to greater respiration of biolabile protein-like and aliphatic DOM. (b) Under increased precipitation in grassland/herbaceous wetlands, more aromatic DOM from the landscape will be transported into surface waters and stable DOM components will be exported to connected riverine systems during flushing periods. (c) Extensive ponding will amplify differences between surface water DOM and the subsurface in grassland/herbaceous wetlands. Thermodynamic constraints will preserve DOM from the landscape and microbial processing will result in unique aliphatic compounds rich in N and S. Reducing conditions will promote respiration via alternate terminal electron acceptors and methanogenesis.

et al., 2018; Mitsch et al., 2013). However, given the importance of wetlands for transporting organic carbon to fluvial systems and greenhouse gas cycling, wetland DOM composition will have important downstream effects as it responds to changes. Projected warming and precipitation patterns will vary across North America (Almazroui et al., 2021; Easterling et al., 2017), making large scale predictions of wetland responses impractical. Instead, we explore regional outcomes of likely warming and precipitation scenarios in forested (southeast Alaska) and grassland/herbaceous (Prairie Potholes) wetland endmembers from this study and consider how their current DOM composition will respond and influence biogeochemical C cycling.

Average air temperatures are predicted to increase across most of North America (Almazroui et al., 2021), which will likely influence DOC decomposition and export from wetlands undergoing substantial warming. For example, increased soil temperature is a dominant control on DOC production and export from connected wetlands in southeast Alaska and during periods of increased lateral flow, which result in high DOC fluxes to the surrounding watersheds (Fellman et al., 2009; D'Amore et al., 2015). Warming may induce greater DOM solubilization from soil organic matter, increasing both DOC concentrations in wetlands as well as DOC mineralization rates and CO_2 production from the decomposition of solubilized biolabile DOM (Fellman et al., 2017; O'Donnell et al., 2016). Thus, if we consider the DOM composition of forested wetlands with high organic matter soil content from this study (sites E, K, L), ambient warming may increase overall bulk DOC concentrations and CDOM in porewaters and surface waters, but decrease available biolabile DOM (Figure 9a). Compositionally, this DOM will be enriched in biostable condensed aromatics and polyphenolics, as these fractions correlate positively with soil organic matter (Table S5 in Supporting Information S1), while biolabile DOM, such as protein-like fluorophores (C5) and aliphatics, may increase initially due solubilization but will likely degrade over short time scales (Guillemette et al., 2013: Figure 9a). DOM oxygenation (O/C, NOSC) may also increase from the decomposition of larger biopolymers (Lehmann & Kleber, 2015; Roth et al., 2019); however, HUP$_{\text{High O/C}}$

compounds did not correlate significantly with soil organic matter at these sites, suggesting they may instead be controlled by vegetation (Table S5 in Supporting Information S1).

Total precipitation is predicted to increase across southeast Alaska, the eastern USA, and the central USA (Easterling et al., 2017; Lader et al., 2020). This includes the Southeast Prairie Potholes region (I, J) where greater precipitation will lead to wetland expansion and ponding that persists into the midsummer dry season (Ballard et al., 2013). Under this precipitation scenario, wetland surface water connectivity to the landscape will increase across grasslands and herbaceous wetlands, likely resulting in greater terrestrial organic matter transport from vegetation and soil (Johnston et al., 2020; Kurek et al., 2023; Majidzadeh et al., 2017; Figure 9b). This is illustrated by positive correlations between the total monthly accumulated precipitation and condensed aromatics, polyphenolics, and $HUP_{High\ O/C}$ compound classes (Table S5 in Supporting Information S1). Along with these aromatic compounds, fresh biolabile DOM input will likely also increase as these DOM fractions are typically coupled in aquatic systems with strong terrestrial influence (Lapierre & del Giorgio, 2014).

Due to constant flushing, bulk DOC and CDOM will likely decrease in standing surface waters as solutes are diluted and persistent DOM compounds are transported via fluvial systems (e.g., CARF formulae, Figure 9b). Extensive ponding will also form a barrier to oxygen diffusion and promote redox stratification between surface waters and deeper subsurface pore spaces where respiration occurs via alternate terminal electron acceptors (D'Angelo & Reddy, 1999; Pester et al., 2012; Figure 9c). This stratification will further amplify differences between porewater and surface water DOM composition as biolabile reduced aliphatic and $HUP_{Low\ O/C}$ compounds are thermodynamically preserved and unique N,S-containing compounds are produced from microbial processing and abiotic sulfurization (Figure 9c). Although preserved in the subsurface, they may become thermodynamically available for respiration as they are transported or introduced to oxic conditions during drying periods, stimulating biological activity (Boye et al., 2017). Furthermore, while overall soil organic matter content and porewater DOC concentrations may increase due to thermodynamic constraints, processing of these reduced carbon pools may provide additional substrates for fermentation and methanogenesis (Lau & del Giorgio, 2020), further increasing the already high CH_4 fluxes from this region (Dalcin Martins et al., 2017).

Many regions, including the Prairie Potholes, will experience concurrent increases in both warming and precipitation (Almazroui et al., 2021; Ballard et al., 2013), meaning that DOC concentrations and DOM composition will be shaped by combined effects of soil warming and saturation. In these regions, DOM cycling would therefore represent a combination of effects from panels A and B (Figure 9) and will be constrained by factors such as specific vegetation type and soil content. However, the extent to which combined warming and precipitation will influence wetland organic matter transport and cycling compared with other anthropogenic impacts such as drainage, agricultural expansion, and urbanization is currently unknown. Therefore, this and other large-scale assessments of wetland DOM will be important for comparing baseline DOC and DOM composition as wetlands respond to changing conditions and potentially mobilize large pools of carbon.

5. Conclusion

This study characterizes DOC and DOM across various temperate USA wetland types and explores their composition with respect to geographic differences. DOC concentrations and aromaticity were similar to those of North American rivers and major tropical-subtropical wetland systems, highlighting their primary terrestrial sourcing and interaction with the surrounding landscape. However, several wetland sites contained key differences in internal DOM sourcing and degradation due to soil properties and hydroclimate. Across the sites, wetland DOM composition was driven by differences in landcover, where aromatic DOM was more prevalent in forested sites, whereas grassland/herbaceous wetlands contained more aliphatic molecular formulae. DOM composition also differed by sampling depth, where surface waters were enriched in oxygenated formulae spanning both high and low-molecular weights in contrast to porewaters which displayed extensive S-content. Furthermore, we identified a group of persistent DOM formulae across all sites, sampling depths, and hydroperiods (i.e., the molecular level signature of wetland DOM), many of which were also found in the largest arctic rivers, highlighting the important contribution of wetland DOM to riverine/coastal carbon export. Finally, increased temperature and precipitation patterns will likely deliver DOC and aromatic DOM into wetlands while amplifying the differences between surface and subsurface processing. As wetlands across the USA experience changes in hydroclimate and land use, the composition and role of DOM will become increasingly important for understanding carbon balance between landscapes, aquatic systems, and the atmosphere.

Conflict of Interest

The authors declare no conflicts of interest relevant to this study.

Data Availability Statement

The authors declare that all data supporting the results of this study are archived in the Open Science Framework (https://osf.io/v86az/; https://doi.org/10.17605/OSF.IO/V86AZ).

References

Almazroui, M., Islam, M. N., Saeed, F., Saeed, S., Ismail, M., Ehsan, M. A., et al. (2021). Projected changes in temperature and precipitation over the United States, Central America, and the Caribbean in CMIP6 GCMs. *Earth Systems and Environment*, 5, 1–24. https://doi.org/10.1007/s41748-021-00199-5

Aukes, P. J., & Schiff, S. L. (2021). Composition wheels: Visualizing dissolved organic matter using common composition metrics across a variety of Canadian ecozones. *PLoS One*, 16(7), e0253972. https://doi.org/10.1371/journal.pone.0253972

Ballard, T., Seager, R., Smerdon, J. E., Cook, B. I., Ray, A. J., Rajagopalan, B., et al. (2013). Hydroclimate variability and change in the Prairie Pothole region, the "duck factory" of North America. *Earth Interactions*, 18(14), 1–28. https://doi.org/10.1175/ei-d-14-0004.1

Battin, T. J., Luyssaert, S., Kaplan, L. A., Aufdenkampe, A. K., Richter, A., & Tranvik, L. J. (2009). The boundless carbon cycle. *Nature Geoscience*, 2(9), 598–600. https://doi.org/10.1038/ngeo618

Behnke, M. I., McClelland, J. W., Tank, S. E., Kellerman, A. M., Holmes, R. M., Haghipour, N., et al. (2021). Pan-Arctic riverine dissolved organic matter: Synchronous molecular stability, shifting sources and subsidies. *Global Biogeochemical Cycles*, 35(4), e2020GB006871. https://doi.org/10.1029/2020gb006871

Boye, K., Noël, V., Tfaily, M. M., Bone, S. E., Williams, K. H., Bargar, J. R., & Fendorf, S. (2017). Thermodynamically controlled preservation of organic carbon in floodplains. *Nature Geoscience*, 10(6), 415–419. https://doi.org/10.1038/ngeo2940

Bridgham, S. D., Cadillo-Quiroz, H., Keller, J. K., & Zhuang, Q. (2013). Methane emissions from wetlands: Biogeochemical, microbial, and modeling perspectives from local to global scales. *Global Change Biology*, 19(5), 1325–1346. https://doi.org/10.1111/gcb.12131

Bridgham, S. D., Megonigal, J. P., Keller, J. K., Bliss, N. B., & Trettin, C. (2006). The carbon balance of North American wetlands. *Wetlands*, 26(4), 889–916. https://doi.org/10.1672/0277-5212(2006)26[889:tcbona]2.0.co;2

Cole, J. J., Prairie, Y. T., Caraco, N. F., McDowell, W. H., Tranvik, L. J., Striegl, R. G., et al. (2007). Plumbing the global carbon cycle: Integrating inland waters into the terrestrial carbon budget. *Ecosystems*, 10(1), 172–185. https://doi.org/10.1007/s10021-006-9013-8

Corilo, Y. E. (2014). *PetroOrg software*. Florida State University. Retrieved from http://www.petroorg.com

Cory, R. M., & McKnight, D. M. (2005). Fluorescence spectroscopy reveals ubiquitous presence of oxidized and reduced quinones in dissolved organic matter. *Environmental Science & Technology*, 39(21), 8142–8149. https://doi.org/10.1021/es0506962

Cory, R. M., Miller, M. P., McKnight, D. M., Guerard, J. J., & Miller, P. L. (2010). Effect of instrument-specific response on the analysis of fulvic acid fluorescence spectra. *Limnology and Oceanography: Methods*, 8(2), 67–78. https://doi.org/10.4319/lom.2010.8.67

Dalcin Martins, P., Hoyt, D. W., Bansal, S., Mills, C. T., Tfaily, M., Tangen, B. A., et al., (2017). Abundant carbon substrates drive extremely high sulfate reduction rates and methane fluxes in Prairie Pothole Wetlands. *Global Change Biology*, 23(8), 3107–3120. https://doi.org/10.1111/gcb.13633

D'Amore, D. V., Edwards, R. T., Herendeen, P. A., Hood, E., & Fellman, J. B. (2015). Dissolved organic carbon fluxes from hydropedologic units in Alaskan coastal temperate rainforest watersheds. *Soil Science Society of America Journal*, 79(2), 378–388. https://doi.org/10.2136/sssaj2014.09.0380

D'Andrilli, J., Silverman, V., Buckley, S., & Rosario-Ortiz, F. L. (2022). Inferring ecosystem function from dissolved organic matter optical properties: A critical review. *Environmental Science & Technology*, 56(16), 11146–11161. https://doi.org/10.1021/acs.est.2c04240

D'Angelo, E. M., & Reddy, K. R. (1999). Regulators of heterotrophic microbial potentials in wetland soils. *Soil Biology and Biochemistry*, 31(6), 815–830. https://doi.org/10.1016/s0038-0717(98)00181-3

Dewitz, J., & US Geological Survey. (2019). National Land Cover Database (NLCD) 2019 products (ver. 2.0, June 2021). *U.S. Geological Survey Data Release, 2021*. https://doi.org/10.5066/P9KZCM54

Dittmar, T., Koch, B., Hertkorn, N., & Kattner, G. (2008). A simple and efficient method for the solid-phase extraction of dissolved organic matter (SPE-DOM) from seawater. *Limnology and Oceanography: Methods*, 6(6), 230–235. https://doi.org/10.4319/lom.2008.6.230

Drake, T. W., Raymond, P. A., & Spencer, R. G. (2018). Terrestrial carbon inputs to inland waters: A current synthesis of estimates and uncertainty. *Limnology and Oceanography Letters*, 3(3), 132–142. https://doi.org/10.1002/lol2.10055

Easterling, D. R., Arnold, J. R., Knutson, T., Kunkel, K. E., LeGrande, A. N., Leung, L. R., & Wehner, M. F. (2017). Precipitation change in the United States.

Fellman, J. B., D'Amore, D. V., Hood, E., & Cunningham, P. (2017). Vulnerability of wetland soil carbon stocks to climate warming in the perhumid coastal temperate rainforest. *Biogeochemistry*, 133(2), 165–179. https://doi.org/10.1007/s10533-017-0324-y

Fellman, J. B., Hood, E., D'amore, D. V., Edwards, R. T., & White, D. (2009). Seasonal changes in the chemical quality and biodegradability of dissolved organic matter exported from soils to streams in coastal temperate rainforest watersheds. *Biogeochemistry*, 95(2–3), 277–293. https://doi.org/10.1007/s10533-009-9336-6

Fellman, J. B., Hood, E., & Spencer, R. G. (2010). Fluorescence spectroscopy opens new windows into dissolved organic matter dynamics in freshwater ecosystems: A review. *Limnology & Oceanography*, 55(6), 2452–2462. https://doi.org/10.4319/lo.2010.55.6.2452

Graeber, D., Tenzin, Y., Stutter, M., Weigelhofer, G., Shatwell, T., von Tümpling, W., et al. (2021). Bioavailable DOC: Reactive nutrient ratios control heterotrophic nutrient assimilation—An experimental proof of the macronutrient-access hypothesis. *Biogeochemistry*, 155(1), 1–20. https://doi.org/10.1007/s10533-021-00809-4

Groeneveld, M., Catalán, N., Attermeyer, K., Hawkes, J., Einarsdóttir, K., Kothawala, D., et al. (2020). Selective adsorption of terrestrial dissolved organic matter to inorganic surfaces along a boreal inland water continuum. *Journal of Geophysical Research: Biogeosciences*, 125(3), e2019JG005236. https://doi.org/10.1029/2019jg005236

Guillemette, F., McCallister, S. L., & del Giorgio, P. A. (2013). Differentiating the degradation dynamics of algal and terrestrial carbon within complex natural dissolved organic carbon in temperate lakes. *Journal of Geophysical Research: Biogeosciences*, 118(3), 963–973. https://doi.org/10.1002/jgrg.20077

Gullian-Klanian, M., Gold-Bouchot, G., Delgadillo-Díaz, M., Aranda, J., & Sánchez-Solís, M. J. (2021). Effect of the use of Bacillus spp. on the characteristics of dissolved fluorescent organic matter and the phytochemical quality of Stevia rebaudiana grown in a recirculating aquaponic system. *Environmental Science and Pollution Research*, *28*(27), 36326–36343. https://doi.org/10.1007/s11356-021-13148-6

Hanley, K. W., Wollheim, W. M., Salisbury, J., Huntington, T., & Aiken, G. (2013). Controls on dissolved organic carbon quantity and chemical character in temperate rivers of North America. *Global Biogeochemical Cycles*, *27*(2), 492–504. https://doi.org/10.1002/gbc.20044

Hansen, A. M., Kraus, T. E., Pellerin, B. A., Fleck, J. A., Downing, B. D., & Bergamaschi, B. A. (2016). Optical properties of dissolved organic matter (DOM): Effects of biological and photolytic degradation. *Limnology & Oceanography*, *61*(3), 1015–1032. https://doi.org/10.1002/lno.10270

Helms, J. R., Stubbins, A., Ritchie, J. D., Minor, E. C., Kieber, D. J., & Mopper, K. (2008). Absorption spectral slopes and slope ratios as indicators of molecular weight, source, and photobleaching of chromophoric dissolved organic matter. *Limnology & Oceanography*, *53*(3), 955–969. https://doi.org/10.4319/lo.2008.53.3.0955

Hendrickson, C. L., Quinn, J. P., Kaiser, N. K., Smith, D. F., Blakney, G. T., Chen, T., et al. (2015). 21 Tesla Fourier transform ion cyclotron resonance mass spectrometer: A national resource for ultrahigh resolution mass analysis. *Journal of the American Society for Mass Spectrometry*, *26*(9), 1626–1632. https://doi.org/10.1007/s13361-015-1182-2

Hensgens, G., Lechtenfeld, O. J., Guillemette, F., Laudon, H., & Berggren, M. (2021). Impacts of litter decay on organic leachate composition and reactivity. *Biogeochemistry*, *154*(1), 99–117. https://doi.org/10.1007/s10533-021-00799-3

Hertkorn, N., Harir, M., Cawley, K. M., Schmitt-Kopplin, P., & Jaffé, R. (2016). Molecular characterization of dissolved organic matter from subtropical wetlands: A comparative study through the analysis of optical properties, NMR and FTICR/MS. *Biogeosciences*, *13*(8), 2257–2277. https://doi.org/10.5194/bg-13-2257-2016

Imbeau, E., Vincent, W. F., Wauthy, M., Cusson, M., & Rautio, M. (2021). Hidden stores of organic matter in northern lake ice: Selective retention of terrestrial particles, phytoplankton and labile carbon. *Journal of Geophysical Research: Biogeosciences*, *126*(8), e2020JG006233. https://doi.org/10.1029/2020jg006233

Jaffé, R., McKnight, D., Maie, N., Cory, R., McDowell, W. H., & Campbell, J. L. (2008). Spatial and temporal variations in DOM composition in ecosystems: The importance of long-term monitoring of optical properties. *Journal of Geophysical Research*, *113*(G4), G04032. https://doi.org/10.1029/2008jg000683

Jaffé, R., Yamashita, Y., Maie, N., Cooper, W. T., Dittmar, T., Dodds, W. K., et al. (2012). Dissolved organic matter in headwater streams: Compositional variability across climatic regions of North America. *Geochimica et Cosmochimica Acta*, *94*, 95–108. https://doi.org/10.1016/j.gca.2012.06.031

Johnston, S. E., Bogard, M. J., Rogers, J. A., Butman, D., Striegl, R. G., Dornblaser, M., & Spencer, R. G. (2019). Constraining dissolved organic matter sources and temporal variability in a model sub-Arctic lake. *Biogeochemistry*, *146*(3), 271–292. https://doi.org/10.1007/s10533-019-00619-9

Johnston, S. E., Striegl, R. G., Bogard, M. J., Dornblaser, M. M., Butman, D. E., Kellerman, A. M., et al. (2020). Hydrologic connectivity determines dissolved organic matter biogeochemistry in northern high-latitude lakes. *Limnology & Oceanography*, *65*(8), 1764–1780. https://doi.org/10.1002/lno.11417

Kassambara, A., & Mundt, F. (2017). Factoextra: Extract and visualize the results of multivariate data analyses. *R package version*, *1*(4), 2017.

Kellerman, A. M., Guillemette, F., Podgorski, D. C., Aiken, G. R., Butler, K. D., & Spencer, R. G. (2018). Unifying concepts linking dissolved organic matter composition to persistence in aquatic ecosystems. *Environmental Science & Technology*, *52*(5), 2538–2548. https://doi.org/10.1021/acs.est.7b05513

Knapp, A. K., Beier, C., Briske, D. D., Classen, A. T., Luo, Y., Reichstein, M., et al. (2008). Consequences of more extreme precipitation regimes for terrestrial ecosystems. *BioScience*, *58*(9), 811–821. https://doi.org/10.1641/b580908

Koch, B. P., & Dittmar, T. (2006). From mass to structure: An aromaticity index for high-resolution mass data of natural organic matter. *Rapid Communications in Mass Spectrometry*, *20*(5), 926–932. https://doi.org/10.1002/rcm.2386

Koch, B. P., & Dittmar, T. (2016). From mass to structure: An aromaticity index for high-resolution mass data of natural organic matter. *Rapid Communications in Mass Spectrometry*, *30*(1), 250. https://doi.org/10.1002/rcm.7433

Kolka, R., Trettin, C., Tang, W., Krauss, K. W., Bansal, S., Drexler, J. Z., et al., (2018). *Terrestrial wetlands* (Vol. 13, pp. 507–567). US Global Change Research Program.

Kothawala, D. N., Murphy, K. R., Stedmon, C. A., Weyhenmeyer, G. A., & Tranvik, L. J. (2013). Inner filter correction of dissolved organic matter fluorescence. *Limnology and Oceanography: Methods*, *11*(12), 616–630. https://doi.org/10.4319/lom.2013.11.616

Kurek, M. R., Garcia-Tigreros, F., Wickland, K. P., Frey, K. E., Dornblaser, M. M., Striegl, R. G., et al. (2023). Hydrologic and landscape controls on dissolved organic matter composition across western North American Arctic lakes. *Global Biogeochemical Cycles*, *37*(1), e2022GB007495. https://doi.org/10.1029/2022gb007495

Kurek, M. R., Poulin, B. A., McKenna, A. M., & Spencer, R. G. (2020). Deciphering dissolved organic matter: Ionization, dopant, and fragmentation insights via fourier transform-ion cyclotron resonance mass spectrometry. *Environmental Science & Technology*, *54*(24), 16249–16259. https://doi.org/10.1021/acs.est.0c05206

Kurek, M. R., Stubbins, A., Drake, T. W., Dittmar, T., MS Moura, J., Holmes, R. M., et al. (2022). Organic molecular signatures of the Congo River and comparison to the Amazon. *Global Biogeochemical Cycles*, *36*(6), e2022GB007301. https://doi.org/10.1029/2022gb007301

Lader, R., Bidlack, A., Walsh, J. E., Bhatt, U. S., & Bieniek, P. A. (2020). Dynamical downscaling for southeast Alaska: Historical climate and future projections. *Journal of Applied Meteorology and Climatology*, *59*(10), 1607–1623. https://doi.org/10.1175/jamc-d-20-0076.1

Lal, R. (2008). Carbon sequestration. *Philosophical Transactions of the Royal Society B: Biological Sciences*, *363*(1492), 815–830. https://doi.org/10.1098/rstb.2007.2185

Lambert, T., Darchambeau, F., Bouillon, S., Alhou, B., Mbega, J. D., Teodoru, C. R., et al. (2015). Landscape control on the spatial and temporal variability of chromophoric dissolved organic matter and dissolved organic carbon in large African rivers. *Ecosystems*, *18*(7), 1224–1239. https://doi.org/10.1007/s10021-015-9894-5

Lapierre, J. F., & del Giorgio, P. A. (2014). Partial coupling and differential regulation of biologically and photochemically labile dissolved organic carbon across boreal aquatic networks. *Biogeosciences*, *11*(20), 5969–5985. https://doi.org/10.5194/bg-11-5969-2014

Lau, M. P., & del Giorgio, P. (2020). Reactivity, fate and functional roles of dissolved organic matter in anoxic inland waters. *Biology Letters*, *16*(2), 20190694. https://doi.org/10.1098/rsbl.2019.0694

Lehmann, J., & Kleber, M. (2015). The contentious nature of soil organic matter. *Nature*, *528*(7580), 60–68. https://doi.org/10.1038/nature16069

Li, Y., Harir, M., Uhl, J., Kanawati, B., Lucio, M., Smirnov, K. S., et al. (2017). How representative are dissolved organic matter (DOM) extracts? A comprehensive study of sorbent selectivity for DOM isolation. *Water Research*, *116*, 316–323. https://doi.org/10.1016/j.watres.2017.03.038

Lu, Q., He, D., Pang, Y., Zhang, Y., He, C., Wang, Y., et al. (2020). Processing of dissolved organic matter from surface waters to sediment pore waters in a temperate coastal wetland. *Science of the Total Environment*, *742*, 140491. https://doi.org/10.1016/j.scitotenv.2020.140491

Majidzadeh, H., Uzun, H., Ruecker, A., Miller, D., Vernon, J., Zhang, H., et al. (2017). Extreme flooding mobilized dissolved organic matter from coastal forested wetlands. *Biogeochemistry*, *136*(3), 293–309. https://doi.org/10.1007/s10533-017-0394-x

Mann, P. J., Spencer, R. G. M., Dinga, B. J., Poulsen, J. R., Hernes, P. J., Fiske, G., et al. (2014). The biogeochemistry of carbon across a gradient of streams and rivers within the Congo Basin. *Journal of Geophysical Research: Biogeosciences*, *119*(4), 687–702. https://doi.org/10.1002/2013jg002442

McKnight, D. M., Boyer, E. W., Westerhoff, P. K., Doran, P. T., Kulbe, T., & Andersen, D. T. (2001). Spectrofluorometric characterization of dissolved organic matter for indication of precursor organic material and aromaticity. *Limnology & Oceanography*, *46*(1), 38–48. https://doi.org/10.4319/lo.2001.46.1.0038

Mitra, S., Wassmann, R., & Vlek, P. L. (2005). An appraisal of global wetland area and its organic carbon stock. *Current Science*, *88*(1), 25–35.

Mitsch, W. J., Bernal, B., Nahlik, A. M., Mander, Ü., Zhang, L., Anderson, C. J., et al. (2013). Wetlands, carbon, and climate change. *Landscape Ecology*, *28*(4), 583–597. https://doi.org/10.1007/s10980-012-9758-8

Moona, N., Holmes, A., Wünsch, U. J., Pettersson, T. J., & Murphy, K. R. (2021). Full-scale manipulation of the empty bed contact time to optimize dissolved organic matter removal by drinking water biofilters. *ACS ES&T Water*, *1*(5), 1117–1126. https://doi.org/10.1021/acsestwater.0c00105

Murphy, K. R., Stedmon, C. A., Graeber, D., & Bro, R. (2013). Fluorescence spectroscopy and multi-way techniques. PARAFAC. *Analytical Methods*, *5*(23), 6557–6566. https://doi.org/10.1039/c3ay41160e

Nahlik, A. M., & Fennessy, M. S. (2016). Carbon storage in US wetlands. *Nature Communications*, *7*(1), 1–9. https://doi.org/10.1038/ncomms13835

O'Donnell, J. A., Aiken, G. R., Butler, K. D., Guillemette, F., Podgorski, D. C., & Spencer, R. G. (2016). DOM composition and transformation in boreal forest soils: The effects of temperature and organic-horizon decomposition state. *Journal of Geophysical Research: Biogeosciences*, *121*(10), 2727–2744. https://doi.org/10.1002/2016jg003431

Ohno, T., Parr, T. B., Gruselle, M. C. I., Fernandez, I. J., Sleighter, R. L., & Hatcher, P. G. (2014). Molecular composition and biodegradability of soil organic matter: A case study comparing two new England forest types. *Environmental Science & Technology*, *48*(13), 7229–7236. https://doi.org/10.1021/es405570c

Osburn, C. L., Wigdahl, C. R., Fritz, S. C., & Saros, J. E. (2011). Dissolved organic matter composition and photoreactivity in prairie lakes of the US Great Plains. *Limnology & Oceanography*, *56*(6), 2371–2390. https://doi.org/10.4319/lo.2011.56.6.2371

Pester, M., Knorr, K. H., Friedrich, M. W., Wagner, M., & Loy, A. (2012). Sulfate-reducing microorganisms in wetlands–fameless actors in carbon cycling and climate change. *Frontiers in Microbiology*, *3*, 72. https://doi.org/10.3389/fmicb.2012.00072

Peuravuori, J., & Pihlaja, K. (1997). Molecular size distribution and spectroscopic properties of aquatic humic substances. *Analytica Chimica Acta*, *337*(2), 133–149. https://doi.org/10.1016/s0003-2670(96)00412-6

Poulin, B. A., Ryan, J. N., Nagy, K. L., Stubbins, A., Dittmar, T., Orem, W., et al. (2017). Spatial dependence of reduced sulfur in Everglades dissolved organic matter controlled by sulfate enrichment. *Environmental Science & Technology*, *51*(7), 3630–3639. https://doi.org/10.1021/acs.est.6b04142

Prigent, C., Papa, F., Aires, F., Rossow, W. B., & Matthews, E. (2007). Global inundation dynamics inferred from multiple satellite observations, 1993–2000. *Journal of Geophysical Research*, *112*(D12), D12107. https://doi.org/10.1029/2006jd007847

Prijac, A., Gandois, L., Jeanneau, L., Taillardat, P., & Garneau, M. (2022). Dissolved organic matter concentration and composition discontinuity at the peat–pool interface in a boreal peatland. *Biogeosciences*, *19*(18), 4571–4588. https://doi.org/10.5194/bg-19-4571-2022

Raeke, J., Lechtenfeld, O. J., Wagner, M., Herzsprung, P., & Reemtsma, T. (2016). Selectivity of solid phase extraction of freshwater dissolved organic matter and its effect on ultrahigh resolution mass spectra. *Environmental Sciences: Processes & Impacts*, *18*(7), 918–927. https://doi.org/10.1039/c6em00200e

R Core Team. (2020). *R: A language and environment for statistical computing*. R Foundation for Statistical Computing. Retrieved from https://www.R-project.org/

Riedel, T., Zak, D., Biester, H., & Dittmar, T. (2013). Iron traps terrestrially derived dissolved organic matter at redox interfaces. *Proceedings of the National Academy of Sciences*, *110*(25), 10101–10105. https://doi.org/10.1073/pnas.1221487110

Rossel, P. E., Vähätalo, A. V., Witt, M., & Dittmar, T. (2013). Molecular composition of dissolved organic matter from a wetland plant (Juncus effusus) after photochemical and microbial decomposition (1.25 yr): Common features with deep sea dissolved organic matter. *Organic Geochemistry*, *60*, 62–71. https://doi.org/10.1016/j.orggeochem.2013.04.013

Roth, V. N., Lange, M., Simon, C., Hertkorn, N., Bucher, S., Goodall, T., et al. (2019). Persistence of dissolved organic matter explained by molecular changes during its passage through soil. *Nature Geoscience*, *12*(9), 755–761. https://doi.org/10.1038/s41561-019-0417-4

Šantl-Temkiv, T., Finster, K., Dittmar, T., Hansen, B. M., Thyrhaug, R., Nielsen, N. W., & Karlson, U. G. (2013). Hailstones: A window into the microbial and chemical inventory of a storm cloud. *PLoS One*, *8*(1), e53550. https://doi.org/10.1371/journal.pone.0053550

Sanderman, J., Hengl, T., & Fiske, G. J. (2017). Soil carbon debt of 12,000 years of human land use. *Proceedings of the National Academy of Sciences*, *114*(36), 9575–9580. https://doi.org/10.1073/pnas.1706103114

Saunois, M., Stavert, A. R., Poulter, B., Bousquet, P., Canadell, J. G., Jackson, R. B., et al. (2020). The global methane budget 2000–2017. *Earth System Science Data*, *12*(3), 1561–1623. https://doi.org/10.5194/essd-12-1561-2020

Savory, J. J., Kaiser, N. K., McKenna, A. M., Xian, F., Blakney, G. T., Rodgers, R. P., et al. (2011). Parts-per-billion Fourier transform ion cyclotron resonance mass measurement accuracy with a "walking" calibration equation. *Analytical Chemistry*, *83*(5), 1732–1736. https://doi.org/10.1021/ac102943z

Seifert, A. G., Roth, V. N., Dittmar, T., Gleixner, G., Breuer, L., Houska, T., & Marxsen, J. (2016). Comparing molecular composition of dissolved organic matter in soil and stream water: Influence of land use and chemical characteristics. *Science of the Total Environment*, *571*, 142–152. https://doi.org/10.1016/j.scitotenv.2016.07.033

Sleighter, R. L., Chin, Y. P., Arnold, W. A., Hatcher, P. G., McCabe, A. J., McAdams, B. C., & Wallace, G. C. (2014). Evidence of incorporation of abiotic S and N into prairie wetland dissolved organic matter. *Environmental Science & Technology Letters*, *1*(9), 345–350. https://doi.org/10.1021/ez500229b

Smith, D. F., Podgorski, D. C., Rodgers, R. P., Blakney, G. T., & Hendrickson, C. L. (2018). 21 tesla FT-ICR mass spectrometer for ultrahigh-resolution analysis of complex organic mixtures. *Analytical Chemistry*, *90*(3), 2041–2047. https://doi.org/10.1021/acs.analchem.7b04159

Sobek, S., Tranvik, L. J., Prairie, Y. T., Kortelainen, P., & Cole, J. J. (2007). Patterns and regulation of dissolved organic carbon: An analysis of 7,500 widely distributed lakes. *Limnology & Oceanography*, *52*(3), 1208–1219. https://doi.org/10.4319/lo.2007.52.3.1208

Spencer, R. G., Aiken, G. R., Dornblaser, M. M., Butler, K. D., Holmes, R. M., Fiske, G., et al. (2013). Chromophoric dissolved organic matter export from US rivers. *Geophysical Research Letters*, *40*(8), 1575–1579. https://doi.org/10.1002/grl.50357

Spencer, R. G., Butler, K. D., & Aiken, G. R. (2012). Dissolved organic carbon and chromophoric dissolved organic matter properties of rivers in the USA. *Journal of Geophysical Research*, *117*(G3), G03001. https://doi.org/10.1029/2011jg001928

Stedmon, C. A., Markager, S., & Bro, R. (2003). Tracing dissolved organic matter in aquatic environments using a new approach to fluorescence spectroscopy. *Marine Chemistry*, *82*(3–4), 239–254. https://doi.org/10.1016/s0304-4203(03)00072-0

Stedmon, C. A., Thomas, D. N., Granskog, M., Kaartokallio, H., Papadimitriou, S., & Kuosa, H. (2007). Characteristics of dissolved organic matter in Baltic coastal sea ice: Allochthonous or autochthonous origins? *Environmental Science & Technology*, *41*(21), 7273–7279. https://doi.org/10.1021/es071210f

Tate, M. T., DeWild, J. F., Ogorek, J. M., Janssen, S. E., Krabbenhoft, D. P., Poulin, B. A., et al. (2023). Chemical characterization of water, sediments, and fish from water conservation areas and canals of the Florida Everglades (USA), 2012 to 2019. *U.S. Geological Survey Data Release*. https://doi.org/10.5066/P976EGIX

Textor, S. R., Guillemette, F., Zito, P. A., & Spencer, R. G. (2018). An assessment of dissolved organic carbon biodegradability and priming in blackwater systems. *Journal of Geophysical Research: Biogeosciences*, *123*(9), 2998–3015. https://doi.org/10.1029/2018jg004470

Tfaily, M. M., Wilson, R. M., Cooper, W. T., Kostka, J. E., Hanson, P., & Chanton, J. P. (2018). Vertical stratification of peat pore water dissolved organic matter composition in a peat bog in northern Minnesota. *Journal of Geophysical Research: Biogeosciences*, *123*(2), 479–494. https://doi.org/10.1002/2017jg004007

Tranvik, L. J., Downing, J. A., Cotner, J. B., Loiselle, S. A., Striegl, R. G., Ballatore, T. J., et al. (2009). Lakes and reservoirs as regulators of carbon cycling and climate. *Limnology & Oceanography*, *54*(6part2), 2298–2314. https://doi.org/10.4319/lo.2009.54.6_part_2.2298

U.S. Department of Agriculture. (1994). *Natural resources conservation service*. STATSGO. Retrieved from https://www.sciencebase.gov/catalog/item/5748b4cae4b07e28b664dda4

United States Department of Agriculture, Natural Resources Conservation Service. (2019). Web Soil Survey. Retrieved from https://websoilsurvey.sc.egov.usda.gov/

USFWS (US Fish and Wildlife Service). (2021). *USFWS (US Fish and Wildlife Service)*. National Wetlands Inventory. Retrieved from https://www.fws.gov/program/national-wetlands-inventory

Vaughn, D. R., Kellerman, A. M., Wickland, K. P., Striegl, R. G., Podgorski, D. C., Hawkings, J. R., et al. (2021). Anthropogenic landcover impacts fluvial dissolved organic matter composition in the Upper Mississippi River Basin. *Biogeochemistry*, *164*, 1–25. https://doi.org/10.1007/s10533-021-00852-1

Weishaar, J. L., Aiken, G. R., Bergamaschi, B. A., Fram, M. S., Fujii, R., & Mopper, K. (2003). Evaluation of specific ultraviolet absorbance as an indicator of the chemical composition and reactivity of dissolved organic carbon. *Environmental Science & Technology*, *37*(20), 4702–4708. https://doi.org/10.1021/es030360x

Wickham, H. (2016). *ggplot2: elegant graphics for data analysis*. Springer.

Wünsch, U. J., Murphy, K. R., & Stedmon, C. A. (2017). The one-sample PARAFAC approach reveals molecular size distributions of fluorescent components in dissolved organic matter. *Environmental Science & Technology*, *51*(20), 11900–11908. https://doi.org/10.1021/acs.est.7b03260

Xian, F., Hendrickson, C. L., Blakney, G. T., Beu, S. C., & Marshall, A. G. (2010). Automated broadband phase correction of Fourier transform ion cyclotron resonance mass spectra. *Analytical Chemistry*, *82*(21), 8807–8812. https://doi.org/10.1021/ac101091w

Yamashita, Y., Scinto, L. J., Maie, N., & Jaffé, R. (2010). Dissolved organic matter characteristics across a subtropical wetland's landscape: Application of optical properties in the assessment of environmental dynamics. *Ecosystems*, *13*(7), 1006–1019. https://doi.org/10.1007/s10021-010-9370-1

Zark, M., & Dittmar, T. (2018). Universal molecular structures in natural dissolved organic matter. *Nature Communications*, *9*(1), 3178. https://doi.org/10.1038/s41467-018-05665-9

Zarnetske, J. P., Bouda, M., Abbott, B. W., Saiers, J., & Raymond, P. A. (2018). Generality of hydrologic transport limitation of watershed organic carbon flux across ecoregions of the United States. *Geophysical Research Letters*, *45*(21), 11–702. https://doi.org/10.1029/2018gl080005

Zhou, Y., Martin, P., & Müller, M. (2019). Composition and cycling of dissolved organic matter from tropical peatlands of coastal Sarawak, Borneo, revealed by fluorescence spectroscopy and parallel factor analysis. *Biogeosciences*, *16*(13), 2733–2749. https://doi.org/10.5194/bg-16-2733-2019

References From the Supporting Information

Blakney, G. T., Hendrickson, C. L., & Marshall, A. G. (2011). Predator data station: A fast data acquisition system for advanced FT-ICR MS experiments. *International Journal of Mass Spectrometry*, *306*(2–3), 246–252. https://doi.org/10.1016/j.ijms.2011.03.009

Boldin, I. A., & Nikolaev, E. N. (2011). Fourier transform ion cyclotron resonance cell with dynamic harmonization of the electric field in the whole volume by shaping of the excitation and detection electrode assembly. *Rapid Communications in Mass Spectrometry*, *25*(1), 122–126. https://doi.org/10.1002/rcm.4838

Chen, T., Beu, S. C., Kaiser, N. K., & Hendrickson, C. L. (2014). Note: Optimized circuit for excitation and detection with one pair of electrodes for improved Fourier transform ion cyclotron resonance mass spectrometry. *Review of Scientific Instruments*, *85*(6), 066107. https://doi.org/10.1063/1.4883179

Climate Engine. (2023). Desert Research Institute and University of Idaho. version 2.1. Retrieved from http://climateengine.org

Cline, J. D. (1969). Spectrophotometric determination of hydrogen sulfide in natural waters. *Limnology and Oceanography*, *14*(3), 454–458. https://doi.org/10.4319/lo.1969.14.3.0454

Emmett, M. R., White, F. M., Hendrickson, C. L., Shi, S. D. H., & Marshall, A. G. (1998). Application of micro-electrospray liquid chromatography techniques to FT-ICR MS to enable high-sensitivity biological analysis. *Journal of the American Society for Mass Spectrometry*, *9*(4), 333–340. https://doi.org/10.1016/s1044-0305(97)00287-0

Hughey, C. A., Hendrickson, C. L., Rodgers, R. P., Marshall, A. G., & Qian, K. (2001). Kendrick mass defect spectrum: A compact visual analysis for ultrahigh-resolution broadband mass spectra. *Analytical Chemistry*, *73*(19), 4676–4681. https://doi.org/10.1021/ac010560w

Huntington, J. L., Hegewisch, K. C., Daudert, B., Morton, C. G., Abatzoglou, J. T., McEvoy, D. J., & Erickson, T. (2017). Climate engine: Cloud computing and visualization of climate and remote sensing data for advanced natural resource monitoring and process understanding. *Bulletin of the American Meteorological Society*, *98*(11), 2397–2410. https://doi.org/10.1175/bams-d-15-00324.1

Kaiser, N. K., McKenna, A. M., Savory, J. J., Hendrickson, C. L., & Marshall, A. G. (2013). Tailored ion radius distribution for increased dynamic range in FT-ICR mass analysis of complex mixtures. *Analytical Chemistry*, *85*(1), 265–272. https://doi.org/10.1021/ac302678v

Kendrick, E. (1963). A mass scale based on CH_2 = 14.0000 for high resolution mass spectrometry of organic compounds. *Analytical Chemistry*, *35*(13), 2146–2154. https://doi.org/10.1021/ac60206a048

Stookey, L. L. (1970). Ferrozine—A new spectrophotometric reagent for iron. *Analytical Chemistry*, *42*(7), 779–781. https://doi.org/10.1021/ac60289a016